KONA Powder and Particle Journal

KONA Powder and Particle Journal No. 42 (2025) 100–120/https://doi.org/10.14356/kona.2025006 Review Paper

The Effect of Process Conditions on Powder Flow Properties for Slow Flow Regimes †

Sina Zinatlou Ajabshir, Diego Barletta * and Massimo Poletto

Dipartimento di Ingegneria Industriale, Università degli Studi di Salerno, Italy

In several industrial units and applications, particulate solids are exposed to peculiar process conditions that significantly affect their flowability. Accurate characterisation and prediction of these effects are crucial for proper design and operation control of the processes. Liquid content, environmental humidity, and temperature can directly modify the type and magnitude of the interparticle forces and, thus, the cohesive behaviour at the bulk scale. This paper reports a critical review of experimental and modelling studies regarding the quantitative assessment of the effect of powder liquid content, environmental gas humidity and temperature on the mechanics of dense particle assemblies. Particular attention is paid to novel setups and experimental protocols that aim to go beyond the limits of standard and commercial instruments. A multiscale approach is followed from the particle level to the bulk level.

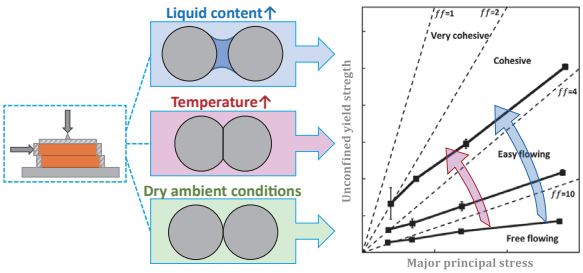

Keywords: powder flow properties, cohesion, liquid content, humidity, temperature, capillary condensation

1. Introduction

The rheology of dense particle assemblies plays a major role not only in several conventional unit operations (storage, handling, mixing, fluidisation, granulation, and milling) but also in more recent applications such as additive manufacturing (Cordova et al., 2020), pharmaceutical dry powder delivery (Price et al., 2002), calcium looping reactors (Durán-Olivencia et al., 2023), concentrated solar thermal technologies (Tregambi et al., 2021), plastic waste valorisation (Kartik et al., 2022), and dry battery manufacturing (Gyulai et al., 2023). Process conditions relevant to different industrial unit operations significantly impact particle interactions and, thus, average bulk flow properties. First, different flow regimes ranging from slow to intermediate and rapid exhibit very different phenomena and, therefore, are described by peculiar models that relate solid stress and velocity fields depending on the relevant strain rates. Boundaries between different regimes were proposed in terms of dimensionless inertial number as the ratio between the time scale associated with the consolidation stress and the time scale of the strain, as summarised in recent comprehensive surveys (Francia et al., 2021; Mort et al., 2015). Therefore, all these regimes will not be covered in this review work. The focus of the present review will be on the effect of significant process parameters such as temperature and liquid content particulate systems in the quasi-static regime.

Several experimental and theoretical studies have demonstrated that the flow behaviour of particulate systems at the bulk level is the macroscopic result of solid–solid interactions and fluid–solid interactions at the microscopic particle level. As a result, a multiscale approach is required.

1.1 Powder flow properties and interparticle forces

Powder flow properties in the quasi-static regime result from the frictional and cohesive interactions of particle assemblies. A macroscopic description of the incipient flow is performed by comparing the state of stress in the granular medium with a plastic yield criterion.

The Mohr circle gives a graphical representation of the distribution of normal stress, σ, and shear stress, τ, in a plane (Fig. 1). The intercepts of the Mohr circle with the σ axis correspond to the major principal stress, σ_1, and the minor principal stress, σ_2, with $\sigma_1 > \sigma_2$. The first attempt to describe the frictional component was made by Coulomb, who treated the solids as a rigid plastic material. According to this theory, in a simple shear problem, powder yielding occurs only when, along a direction, the shear stress reaches a limit value related to the normal stress:

$$\tau = \sigma \tan\phi + c \tag{1}$$

where c is the material cohesion and ϕ is the angle of

† Received 10 June 2023; Accepted 8 November 2023
J-STAGE Advance published online 17 March 2024
* Corresponding author: Diego Barletta;
Add: Via Giovanni Paolo II 132, I-84084 Fisciano SA, Italy
E-mail: dbarletta@unisa.it
TEL: +39-089-96-2499

internal friction. Different mathematical functions accounting for the curvature of the yield locus have been proposed, such as the Warren Spring equation (Orband and Geldart, 1997), but the Coulomb equation remains the most used for its simplicity.

This approach can be generalised to the three-dimensional case in terms of a yield criterion, which indicates the limit stress state corresponding to powder yielding. When cohesion cannot be neglected, the material's cohesive strength can be derived for compressive deformation along one principal direction, assuming that negligible stress is applied along the orthogonal principal directions or, alternatively, for traction deformation. The corresponding values are the unconfined yield strength, f_c, and the uniaxial tensile strength, σ_t, as shown in **Fig. 1**. A common representation of flowability is presented in terms of a plot of f_c vs σ_1, referred to as flow function, which can be compared to the flowability class bounded by constant values of the flow factor, $ff_c = \sigma_1/f_c$, according to the classification proposed by Jenike (1964) and completed by Tomas and Schubert (1985) (**Fig. 2**).

Several defined consolidation methods, including shear testers, tensile testers, and rheometers, have been developed to measure bulk powder flow properties, as recently surveyed by Barletta et al. (2019). There are open issues for further scientific research and technical development regarding the characterisation of small powder samples under low consolidation stress (below 1 kPa) (Ghadiri et al., 2020).

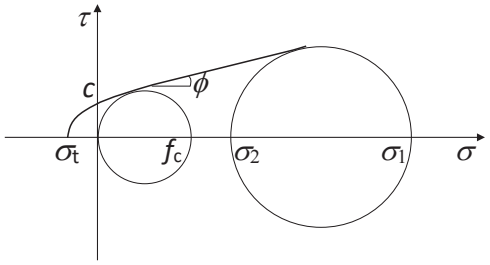

Fig. 1 Mohr-Coulomb analysis on a yield locus to derive powder flow properties.

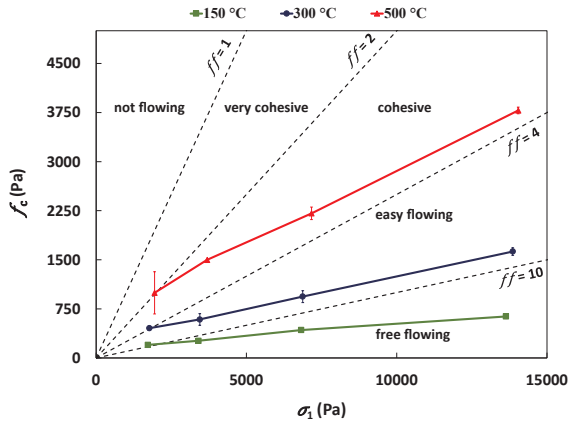

Fig. 2 Flow functions of zeolite T804 at changing temperatures (150, 300 and 500 °C) ranked according to the Jenike flowability classification. Reprinted from Ref. (Zinatlou Ajabshir et al., 2022) under the terms of the CC BY-NC-ND 4.0 license. Copyright: (2022) The Authors, published by Elsevier.

Interparticle forces affecting bulk-scale behaviour are of three main types: van der Waals, capillary and electrostatic forces (Seville et al., 1997). Their intensity is conveniently related to the gravitational force acting on a single particle of the reference size by the dimensionless granular Bond number (Capece et al., 2015, 2016; Castellanos, 2005).

The direct measurement of interparticle adhesive forces appeared challenging; the pull-off experiment with atomic force microscopy was extensively used, but the results are often affected by limited repeatability mainly due to particle surface roughness and asperities, causing wide dispersion of the characteristic size of the interparticle contact and, therefore, of the resulting force (Castellanos, 2005; Rabinovich et al., 2000a).

A theoretical link between the forces at the particle level and the strength of the material at the bulk level can be derived for spherical particles assuming a simplified isostatic state of stress (Rumpf, 1962). This approach has often been applied to estimate the average values of interparticle forces from bulk-scale experimental data (Sofia et al., 2018; Tomas, 2003). In this case, the role of nanoscale asperities must also be properly accounted for to obtain correct quantification (Jallo et al., 2012; LaMarche et al., 2016; Rabinovich et al., 2000b).

2. Effect of liquid content and environmental humidity

2.1 Liquid content

By adding water, moisture, or any other liquid to the powder sample, liquid bridges can form between particles, giving rise to capillary interparticle forces (Mason and Clark, 1965). However, the intensity of capillary forces does not increase monotonically with increasing liquid amount because different liquid distributions arise depending on the liquid saturation amount (Pietsch et al., 1969), which is defined as the volumetric fraction of interparticle voids occupied by the liquid and can be derived from the liquid content on a dry basis, x_w, as follows:

$$S = \frac{1-\varepsilon}{\varepsilon}\frac{\rho_s}{\rho_l}x_w \tag{2}$$

where ε is the volumetric fraction of interparticle voids in the powder, ρ_s is the particle density and ρ_l is the liquid density. In fact, by progressively increasing S, isolated liquid bridges between neighbouring particles can first form (pendular state); then, liquid bridges and liquid menisci on the particle surface roughness co-exist (funicular state); finally, the liquid fills all the available interparticle voids (capillary state) (**Fig. 3**) (Chen and Roberts, 2018; Coelho

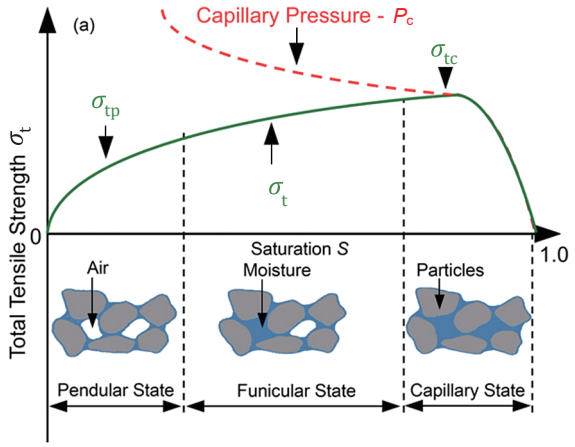

Fig. 3 Tensile strength at increasing saturation. Adapted with permission from Ref. (Chen and Roberts, 2018). Copyright: (2018) Elsevier.

and Harnby, 1978a; Pietsch, 1968). Moreover, the spatial distribution of interparticle voids depends on the particle size distribution, particle shapes, and packing level and thus plays an important role in the capillary networks and on the effective saturation level, as highlighted by 2D and 3D images obtained by X-ray microtomography (Badetti et al., 2018; Louati et al., 2017). The presence of liquid can play a role in the formation of interparticle solid bridges. This phenomenon, referred to as caking, not covered in this paper, is deeply surveyed in the literature (Zafar et al., 2017).

The effect of the presence of liquid in the interparticle voids on cohesive powder properties was investigated using tensile testers, shear cells, and rheometers.

2.1.1 Measurement of the tensile strength and modelling

Experimental studies on the tensile strength of wet powder samples, by direct measurement or by split-cell testers (Eaves and Jones, 1972a, 1972b; Pierrat and Caram, 1997a; Pietsch et al., 1969; Schubert et al., 1975) or derivation from yield loci (Louati et al., 2017), highlighted different behaviours depending on the liquid content and the dry powder properties. Generally, for coarse or fine inorganic powders (particle size distribution, PSD, between 30 and 350 μm) not showing cohesive strength under dry conditions, an increase of the tensile strength was observed with increasing liquid content until a plateau was reached for a range of values of the amount of liquid and then, for much higher liquid saturation, a further significant rise of the strength was registered (Eaves and Jones, 1972a; Louati et al., 2017; Schubert, 1984). This result was explained by a physical interpretation based on the transition between different saturation states and the consequent effect on the forces acting at the particle level.

The tensile strength σ_t can be estimated at low saturation levels, assuming a pendular state, using the Rumpf equation:

$$\sigma_{tp} = (1-\varepsilon)\frac{kF_c}{\pi d^2} \tag{3}$$

where F_c is the capillary force, k is the coordination number, and d is the mean particle size (Pietsch et al., 1969; Rumpf, 1962).

For very high saturation levels, particles are surrounded by the liquid in the capillary state; thus, the tensile strength is proportional to the capillary pressure, P_c, by a factor equal to the saturation:

$$\sigma_{tc} = SP_c \tag{4}$$

For intermediate saturation levels corresponding to the funicular state, both contributions are present with a weighing factor that depends on the saturation value:

$$\sigma_t = \sigma_{tp}\frac{S_2 - S}{S_2 - S_1} + \sigma_{tc}\frac{S - S_1}{S_2 - S_1} \tag{5}$$

where S_1 is the critical liquid saturation between the pendular and the funicular state while S_2 is the critical liquid saturation between the funicular and capillary states. S_1 can vary between 0.25 and 0.5, while S_2 is generally larger than 0.9 (Pierrat and Caram, 1997a).

The capillary pressure P_c, present in **Eqn. (4)**, can be estimated by the following equation:

$$P_c = a'\frac{1-\varepsilon}{\varepsilon}\frac{\gamma}{d} \tag{6}$$

where γ is the liquid surface tension and a' is a constant depending on the particulate material, assuming a value between 6 and 8 and between 1.9 and 14.5 for narrow and wide particle size distributions, respectively (Schubert, 1984).

For particles below 1 mm, the capillary force F_c, appearing in **Eqn. (3)**, can be estimated as the sum of two main contributions: the first is the axial component of the surface tension force, F_c, at the interface between solid, liquid, and gas, which always results in an attractive force; the second is the force, F_p, caused by the change in pressure in the liquid bridge with respect to the atmospheric value due to the curvature of the liquid interface:

$$F_c = F_s + F_p \tag{7}$$

Assuming a saddle-shaped liquid bridge according to the Laplace–Young equation, the pressure difference between air and liquid is given by

$$\Delta p = \gamma\left(\frac{1}{R_1} - \frac{1}{R_2}\right) \tag{8}$$

where R_1 and R_2 are the characteristic curvature radii of a liquid bridge (one is convex and is related to the narrowest circular cross-section of the bridge; the other approximates the curvature radius of the toroidal concavity, **Fig. 4**). The

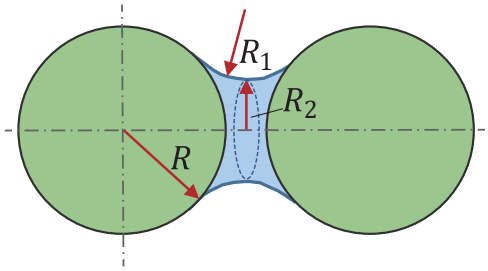

Fig. 4 Liquid bridge and characteristic radii in **Eqn. (8)**.

pressure force turns out to be generally attractive because a pressure reduction is established in the liquid bridge (in fact $R_2 > R_1$), but it could be repulsive if a pressure increase arose.

Gradually increasing the liquid content to the funicular state, the attractive force F_p due to suction at the gas–liquid interface can reduce the distance (Chen and Roberts, 2018) between the particles connected by the liquid and create an uneven spatial distribution of the interparticle voids. Generally, the resulting average bondage also reduces (Louati et al., 2017).

In the pendular regime, several theoretical equations for the capillary force proposed in the literature differ for the assumptions made regarding the size and shape of the two particles in contact with the liquid bridge and the geometry of the liquid bridge itself, including the liquid contact angle of the liquid on solid surfaces. Equations were more easily derived by assuming spherical particles, zero contact angles, and a toroidal bridge. The general form of the total capillary force is

$$F_c = K\gamma r \tag{9}$$

where r is a characteristic curvature radius of the particle surface in contact with the liquid bridge, and K is a complex function of several geometrical parameters of the liquid bridge, such as the interparticle distance, the half-angle of the liquid bridge (also referred to as filling angle), and the contact angle. More details on capillary forces between surfaces of different shapes (between sphere and sphere, between sphere, cone, cylinder and plane), with and without microscale roughness, can be found elsewhere (Butt and Kappl, 2009).

The combination of **Eqns. (3)** to **(9)** predicts the possible existence of the plateau of the tensile strength experimentally observed in the pendular regime. Moreover, following the analysis for a single liquid bridge forming between two equal spherical particles, the capillary force may increase up to a plateau value with increasing filling angle, which is related to the overall liquid saturation (Weigert and Ripperger, 1999) since the contribution due to the surface tension rises monotonically while the force due to the suction initially assumes increasing positive values (attractive) then, after reaching a maximum, decreases down to negative values (repulsive) for a range of values of the ratio between the interparticle distance and the particle size between 5×10^{-2} and 0.5 (Pierrat and Caram, 1997a; Pietsch and Rumpf, 1967). Moreover, by increasing the liquid saturation in a powder sample, the average number of liquid bridges per particle increases until a roughly constant value is reached in the pendular regime (Kohonen et al., 2004). However, micro cracks and roughness on the particle surface could absorb liquid from the surface, reducing the probability of liquid bridge formation and, thus, the capillary force (Johanson et al., 2003).

Peculiar observations have been made for very fine powders (PSD mostly below 15 μm) with cohesive properties at very low moisture contents (Eaves and Jones, 1972a; 1972b). In fact, the tensile strength reaches a maximum value at a very limited amount of liquid (lower than 1–2 % w/w dry basis), then decreases with increasing liquid amount up to 50 % of the maximum value for liquid content between 5 % and 10 % w/w dry basis. This trend was interpreted by Eaves et al. (1972b), assuming that free water on the particle surface could swamp microcontacts between particles and, thus, cause a reduction in the intensity of van der Waals forces not balanced by the increase in capillary forces. In fact, this trend is in qualitative agreement with the prediction that the capillary force decreases as a function of the filling angle for the case where the ratio between the interparticle distance and the particle size tends to zero for equal spherical particles (Pietsch and Rumpf, 1967).

2.1.2 Measurement of the yield loci

Direct shear tests with translational and rotational cells confirmed the effect of capillary forces on bulk flow properties on a range of fine powders with increasing content of different liquids such as water, aqueous solutions, and oil (Althaus and Windhab, 2012; Badetti et al., 2018; Emery et al., 2009; Johanson et al., 2003; Louati et al., 2017; Lu et al., 2018; Pierrat et al., 1998; Pierrat and Caram, 1997a).

Inspection of experimental yield loci highlighted that the cohesion increased with increasing liquid content in the low range (<5–10 % w/w), whereas the internal friction angle remained almost unchanged. The increase in cohesion appears to be more pronounced for higher consolidation stress values (Johanson et al., 2003; Louati et al., 2017). A quantitative prediction of the cohesion increase was proposed with the so-called theory of shift of a linearised yield locus, assuming a constant value of the angle of friction ϕ (Pierrat et al., 1998). The shift of the yield locus is estimated in terms of the reduction of the normal stress, $\Delta\sigma$, providing the same shear strength in the dry condition. An expression of $\Delta\sigma$ as a function of the changes in the tensile strength, $\Delta\sigma_t$, is proposed:

$$\Delta\sigma = \Delta\sigma_t \frac{1+\sin\phi}{2\sin\phi} \tag{10}$$

This equation shows that a wet powder yield locus shifts to the left compared to that for dry conditions. $\Delta\sigma_t$ can be directly measured by a split cell or derived from model predictions according to **Eqn. (5)**.

An irregular particle shape can drive a different effect of the liquid presence on the cohesive strength (Emery et al., 2009). In fact, for needle-shaped particles (e.g. aspartame powders), an optimal moisture content value was found to improve flowability. By increasing the liquid content, an improvement of flowability (increase of the flow factor or decrease of cohesive strength) was observed because of the formation of round-shaped agglomerates, while going beyond this critical moisture value (e.g. 5 % w/w), the flowability decreased because of increments of capillary forces of liquid bridges between agglomerates. In contrast, for particles ranging from spheres to elongated shapes with smooth edges (e.g., Hydroxypropyl Methylcellulose powders), a more cohesive behaviour was obtained by increasing the water content (5 % w/w). Then, an improvement in flowability for higher moisture contents (10 % w/w) was interpreted, considering the possible lubricating effect of a thick layer of liquid on the particle surface.

Prediction of the effect of moisture on powders consisting of porous particles appeared to be more challenging because it is necessary to estimate the amount of liquid penetrating the particle porosity and, thus, not available for the formation of liquid bridges (Lu et al., 2018).

A more complete survey of the experimental and modelling results on the effect of liquid content is reported in **Table 1**.

2.2 Effect of capillary condensation

Liquid water or moisture content in powders can be caused by the exposition of the sample to a humid atmosphere and the consequent capillary condensation leading to liquid bridge formation (Coelho and Harnby, 1978b). Such phenomena typically occur in storage containers and process units such as dryers and fluidised bed reactors. Capillary condensation was studied by directly observing liquid bridges between particles and indirectly measuring the induced cohesive properties at the bulk level.

Capillary condensation is possible for the reduction of the vapour pressure of water due to the reduced pressure within the liquid bridge determined by the surface tension acting over a curved concave interfacial surface with air. The modified vapour pressure is described by the Kelvin equation:

$$p_s = p_{s0} \exp\left[-\frac{M_w \Delta p}{\rho_l R_g T}\right] \tag{11}$$

where p_{s0} is the vapour pressure of the liquid, p_s is the vapour pressure over a curved surface, M_W is the molecular weight of water, R_g is the universal gas constant, and T is temperature. Δp is the pressure difference between gas and liquid, as predicted by the Laplace–Young equation, **Eqn. (8)**.

As a result, regardless of the relative (air) humidity (*RH*), condensation occurs in liquid bridges or other liquid menisci with concave curvature radii small enough to provide a decrease in the liquid pressure sufficient to lower p_s below the water partial pressure. At equilibrium, it is

$$RH = \frac{p_s}{p_{s0}} = \exp\left[-\frac{M_w \Delta p}{\rho_l R_g T}\right] \tag{12}$$

Experiments using a simplified translational shear cell were performed on various powders with different PSD limits and particle shapes under controlled air humidity conditions in a climatic chamber (Elbirli et al., 1982). The results highlighted that the effect of humidity on the powder shear strength varies significantly with the geometrical features of the particle surface and the resulting curvature of interparticle contact points, as well as with the surface hydrophilic/hydrophobic properties. In fact, for silane-coated glass beads and TiO_2 particles with almost spherical contact points (PSD range 125–190 μm) and hydrophobic surfaces, the effect of air humidity was nearly negligible, and a small reduction in cohesive strength was observed for $RH < 90$ %. These results do not contradict the theoretical prediction of the capillary force due to capillary condensation at increasing *RH* on spherical particles, obtained by combining the Kelvin and Laplace–Young equations with the capillary force equation as the sum of the surface tension force and the pressure force (Coughlin et al., 1982). Instead, for powder with more irregularly shaped particles and rough surfaces, such as amorphous silica (PSD range 0.4–15 μm), an increase in cohesive strength was found with increasing *RH*. However, different trends were observed, including the observation of a minimum or maximum strength for critical humidity values. Interpretations can be attempted on a case-by-case inspection of SEM images of the particles, revealing very irregular shapes, including flat sides, elongated shapes, and eventually agglomerates of particles that play a complex role in the contact point distribution and effective capillary condensation.

The role of the roughness of the particle surface on capillary condensation has been widely studied by several authors on theoretical grounds. The presence of asperities must be taken into account when modelling liquid condensation at the contact point between a conical asperity and a flat surface, highlighting the prevailing contribution of the capillary suction force (Coughlin et al., 1982). The resulting adhesive force increased with increasing relative humidity (*RH*). A more significant increase was predicted for larger cone half-angle values. However, because the characteristic size of the calculated liquid bridge did not exceed a few nanometers, a length comparable with the molecular scale, until $RH > 0.3$, quantitative values are affected by

Table 1 Overview of case studies on the effect of liquid content on powder strength, friction and cohesion (chronological order).

Reference	Liquid content (%)	Powders/Tester/Properties	Main results
(Pietsch et al., 1969)	0–21 (Water)	Limestone/agglomerate TS tester/TS	TS increases with moisture up to a plateau and then continues to increase. Model for pendular and capillary regimes.
(Eaves and Jones, 1972a)	0–17 (Water)	Sodium chloride/split-cell TS tester/TS	PSD influence: for coarse powders, TS increases with moisture up to a plateau; for fine powders, a maximum value is found at a very limited amount of liquid (<1–2 % w/w dry basis), then decreases with increasing liquid amount up to 50 % for liquid content between 5 % and 10 % w/w dry basis.
(Eaves and Jones, 1972b)	0–15 (Water)	Ca phosphate, glass beads, potassium chloride/split-cell Parfitt TS tester/TS	The TS of calcium phosphate is almost constant with moisture due to porous particles.
(Pierrat and Caram, 1997b)	0.7–8 (Water, surfactants)	Glass beads/Parfitt TS tester with a larger split cell/YL	TS increases with liquid content up to a plateau in the pendular regime and strongly depends on powder bed voidage; a correlation is proposed.
(Pierrat et al., 1998)	1.3–25 (Water)	Crushed limestone, Super D catalyst, Leslie coal, glass beads/translational ST/YL	Increase in cohesion with moisture. AIF is almost independent of moisture. Proposed equation for the yield locus shift with moisture.
(Johanson et al., 2003)	0–0.12 (Oil)	Glass beads/Schulze ST/FF	Increase in UYS with oil content. UYS decreases with increasing particle size.
(Richefeu et al., 2006)	0–3 (Distilled water)	Sand grains, glass beads/ Translational ST/YL	Increase of cohesion to a plateau value with moisture.
(Althaus and Windhab, 2012)	18–30 (Aq. solution with dextrin)	Glass beads and silica/ Schulze ring ST/YL	Cohesion and uniaxial TS increase with moisture and as a function of the different identified saturation regimes.
(Althaus et al., 2012)	16, 18, 20 (Aq. solution with dextrin)	Glass beads/Schulze RST/YL	Limited effect of dextrin concentration on YL. A semi-empirical model linking capillary forces and YL.
(Louati et al., 2017)	0, 0.5, 3.5, and 40 (PEG)	Glass beads/Hosokawa MPT, Schulze RST/AOR, YL	TS is more affected by liquid at consolidation stress > 4 kPa. X-ray tomographic images highlight saturation levels.
(Lu et al., 2018)	1.6–29 (Water)	Pulverized coal/Hosokawa MPT, Freeman FT4 Powder Rheometer/AOR, HR, Carr flowability index, Cohesion, Angle of internal friction, FF	Increase in AOR and HR with moisture. Increase in cohesion and decrease in flowability for moisture higher than a critical value (15–20 % w/w).
(Badetti et al., 2018)	1.5–7.5 (Silicone oil)	Polystyrene beads/Stress-controlled rheometers with an annular shear cell/Apparent friction coefficient	The apparent friction coefficient (τ/σ) increases with moisture and with the inertia number. Proposed equation for apparent friction coefficient as a function of reduced pressure and inertia number.
(Chen et al., 2018)	3.5–17 (Water)	Coal, Bauxite, Iron ore/Jenike ST/TS, FF	FF vertical shift (flowability decreases) with moisture. Proposed modification of the flowability classification for high consolidation.

significant uncertainty at low *RH*. An extension of the analysis to a couple of generic curved asperities in contact highlighted the significant effect of curvature on the acting force. For smooth micrometric spherical particles, the capillary force is mainly proportional to the particle radius and is not significantly affected by the relative humidity (Bocquet et al., 1998). Instead, capillary condensation is relevant to asperities of nanometric size, comparable to the Kelvin length, that is, the concave curvature radii allowing condensation at $RH \approx 0.1$ (Butt, 2008), explaining the onset of capillary forces. A more comprehensive model, experimentally validated by AFM measurements, has been

proposed for an asperity in contact with a larger spherical particle (Rabinovich et al., 2002). The results revealed that adhesive forces increased and the critical relative humidity decreased with decreasing root mean square roughness. An extension of this analytical approach also considered the roughness distribution on irregularly shaped particles (Butt, 2008). The predicted capillary force increased with *RH* up to a maximum value close to that of the force estimated for a smooth particle (**Fig. 5**). The complete picture of the physical interpretation is that at low *RH*, a single capillary bridge forms by condensation between close nanometric asperities of particles in contact and, therefore, the van der Waals force that is proportional to the overall particle size (order from tens to few hundreds microns) prevails. At intermediate *RH*, the number of capillary bridges increases and the sum of acting capillary force increases. At high *RH*, liquid water fills all the voids between asperities to obtain a large capillary meniscus with a larger curvature radius comparable with the overall particle size. This situation corresponds to the maximum intensity of the capillary force (**Fig. 6**) (Butt and Kappl, 2009).

Experiments performed at the bulk level confirmed the conclusions of force analysis at the particle level. In fact, powder cohesion varied only for air humidity values higher than a critical value by analysing the results of shear tests (Elbirli et al., 1982; Karde and Ghoroi, 2015; Landi et al., 2011; Salehi et al., 2021; Stevens et al., 2009; Teunou and Fitzpatrick, 1999), torque and energy measurements in rheometers (Groen et al., 2020; Landi et al., 2012; Lu et al., 2017; Marchetti et al., 2022), and flowability indices in rotating drums (Lumay et al., 2016).

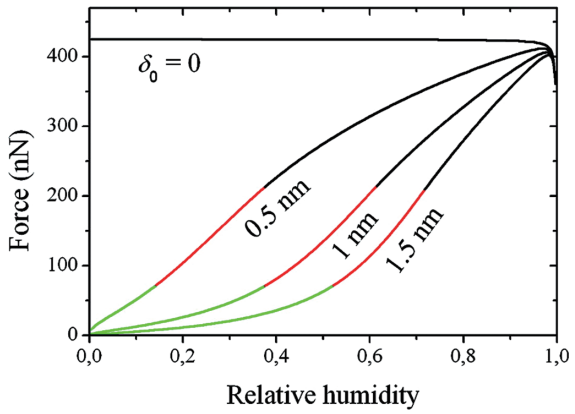

Fig. 5 Capillary forces at various humidity amounts and surface roughness. Same rough spheres with 1 μm radius and constant contact angle $\theta = 20°$. δ_0 is the characteristic roughness. Reprinted with permission from Ref. (Butt, 2008). Copyright: (2008) Elsevier.

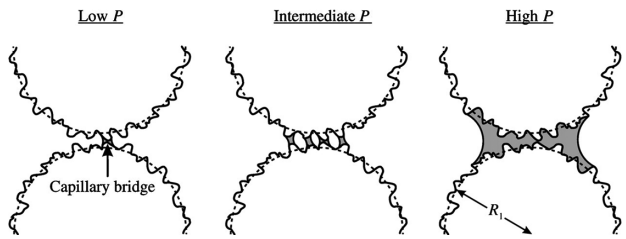

Fig. 6 Capillary bridge patterns between particles with asperities at increasing relative humidity. Reprinted with permission from Ref. (Butt and Kappl, 2009). Copyright: (2009) Elsevier.

For instance, the results of shear tests on glass beads previously conditioned in a fluidised state by humid air showed an increase in cohesion for $RH > 70$ %, while the angle of internal friction was less affected (Landi et al., 2011). Moreover, by considering the presence of asperities with a curvature radius equal to about one hundred of the bead radius (two samples with 50 μm and 90 beads μm mean size), predictions of the tensile strength by a model combining the Rumpf, Laplace–Young, and Kelvin equations showed good agreement with the values derived from experimental yield loci. A tiny fraction of the condensed moisture between particles could form capillary bridges that play an active role in increasing the powder's cohesion.

As mentioned above for the interparticle forces, relative humidity also affects the unconfined yield strength of powders, depending not only on the particle size and shape but also on the hydrophilic/hydrophobic properties of the particle surface (Karde and Ghoroi, 2015; Stevens et al., 2009). In fact, the moisture content and cohesive strength of hydrophobic ibuprofen powder did not increase with *RH*. In contrast, the increase in the unconfined yield strength of hydrophilic starch and Avicel powders was directly correlated with the measured specific surface energy component increasing at *RH* higher than a critical value (**Fig. 7**). At lower *RH* values, cohesive strength was correlated with the Lifshitz–van der Waals forces due to the dispersive surface energy component. The coexistence of electrostatic charging may explain the minimum unconfined yield strength of starch powder by a possible reduction of electrostatic forces with increasing *RH*.

The cohesion force between particles in different ranges of air relative humidity could provide interesting results. In the range below the critical air relative humidity, particle–particle friction might generate electrostatic forces, which cause cohesive forces between the particles (Harnby et al., 1987; Lumay et al., 2016). In contrast, above the critical air relative humidity, the condensed air moisture determines the cohesion forces (Landi et al., 2011; Lumay et al., 2016). The tensile strength and adhesion forces between particles increase as the relative humidity content increases. At the same time, the consolidation pressures could vary the contribution of the adhesion force. For instance, capillary forces play an important role at low consolidation pressures, but contact forces prevail at high consolidation pressures (Karde et al., 2017).

Table 2 reports a wider overview of the experimental and modelling studies on the effect of air humidity.

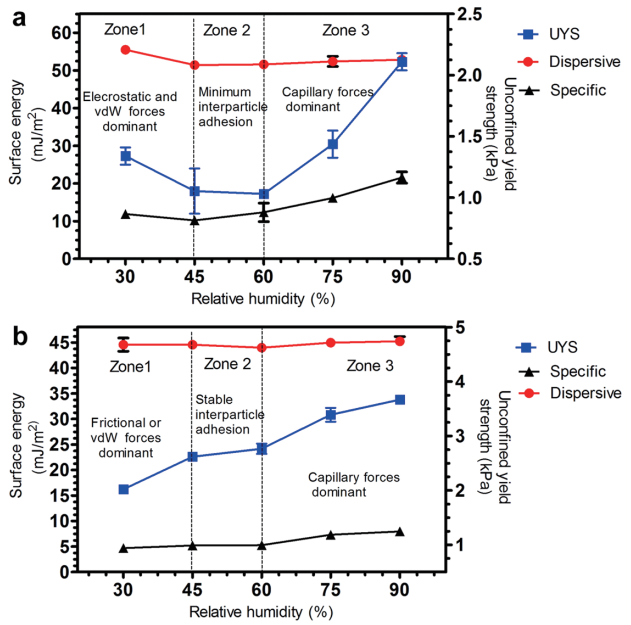

Fig. 7 Correlation between unconfined yield strength (UYS), dispersive and specific surface energy components for **a)** starch powder and **b)** Avicel powder. Reprinted with permission from Ref. (Karde and Ghoroi, 2015). Copyright: (2015) Elsevier.

3. Effect of temperature

The effect of temperature on the mechanical properties of powders was tested by considering the direct measure of binary interparticle forces at the microscopic level and bulk scale properties at defined bulk consolidation, such as tensile strength or shear testing properties.

3.1 Direct measurement of the interparticle forces

3.1.1 Experimental setup and procedures

The direct measurement of interparticle forces at changing temperatures is a complex task, and the literature reports only the high-temperature micro-force balance developed by Pagliai et al. (Pagliai et al., 2004). The setup included a system of micromanipulators to set the position of two particles in an electric oven to heat the system to 1000 °C, where a camera allowed image recording for visual observation. The relative motion between the couple of tested particles was regulated by a linear displacement actuator moving one of the two particles. The pulling force between the two particles in contact was derived from the cantilever deflection of a calibrated bending strip mounted on the static micromanipulator while pulling.

A micromanipulation system for measuring interparticle forces under controlled humidity and temperature was also developed by Haider et al. (2012) to measure the increase of adhesion force between amorphous maltodextrin particles when the temperature approached the glass transition temperature. The mechanism involved is related to the desired particle agglomeration, which is beyond the scope of this review.

3.1.2 Main observed phenomena

Pagliai et al. (2004) performed measurements on particles of E-cat powder (a powder similar to those used in fluid catalytic cracking reactors). This powder was withdrawn from the process, where it exhibited defluidization at high temperatures. The change in interparticle forces with increasing temperature was observed with a liquid bridge forming between the tested particles at 90 °C due to low melting compounds. However, the low surface tension of the formed liquid made the intensity of the capillary force not very high. In fact, a hydrocarbon liquid phase is formed. The liquid evaporated at 180 °C and up to 300 °C, and a solid bridge formed between the two particles. Correspondingly, the measured force increased significantly.

3.2 Experimental setup and procedures for the bulk solids properties

The effect of temperature on bulk flow properties was investigated by conventional characterisation techniques in different apparatuses properly modified for high-temperature experiments.

3.2.1 Direct evaluation of the tensile strength

Several studies have exploited the split cell tensile testers developed for tests up to 1100 °C by Kamiya et al. (2002b). This apparatus (**Fig. 8a**) was made of a circular vertically split cell consisting of a fixed part and a horizontally moving part suspended by a very thin metal plate. The cell was heated by radiation from the top and bottom in a furnace purposely prepared. The cell was made of silica glass to limit thermal expansion. The experimental procedure was similar to a conventional tensile test, with the only difference being the heating and monitoring of the powder sample temperature by a thermocouple. It consisted of a vertical consolidation step with a normal stress of 2.5 kPa and a successive tensile failure step during which the pull-off force and displacement of the movable part were measured.

Different apparatuses for a vertical uniaxial tensile test have been recently proposed (Liu et al., 2022; Luan and You, 2015). In the high-temperature solid bridge force device (Luan and You, 2015) (**Fig. 8b**), the ash sample was divided into two parts, which were separately heated in two cylindrical cells at high temperatures between 750 °C and 1250 °C and then put in contact under vertical compressive stresses between 9.5 and 19.9 kPa for a period between 1 and 20 min. After this phase, the two cylinders were vertically separated by a traction motor, and the tensile force was measured. Different specimen preparations were proposed by Liu et al. (2022): a coal ash powder sample was extruded through a cylindrical die under 20 MPa pressure, then it was vertically suspended between two clamping tools and heated at varying temperatures between ambient and 1200 °C for 1 h. Finally, the tensile force to obtain the

Table 2 Overview of case studies on the effect of air humidity on powder strength, friction, and cohesion (chronological order).

References	*RH* (%)	Powders/Tester/Properties	Main results
(Elbirli et al., 1982)	10–96	TiO_2, glass beads, polycarbonate, amorphous silica, and alumina/translational ST/YL	The effect of humidity on cohesive strength varies with particle shape, surface, hydrophilic/hydrophobic properties, surface roughness, and material hardness.
(Harnby et al., 1987)	11–87	Glass beads/Hosokawa MPT/bulk density, HR	The aerated and tapped bulk density slightly decreases with *RH*. Fluctuating trend in HR.
(Teunou and Fitzpatrick, 1999)	0–97	Food powders (Flour, skim-milk, tea, whey-permeate)/RST/FF	General increase in UYS with *RH* except for flour powder. Food powder composition and wide PSD affect interaction with water. Caking at high *RH*.
(Stevens et al., 2009)	20, 50, 80	Aluminium powder (as received and surface modified)/Schulze RST/FF	Particle coating mitigates the *RH* impact, especially for low hydrophobicity. Further water adsorption did not affect the capillary forces and UYS. Higher humidity may induce lubrication, leading to a reduction in particle friction and lower UYS.
(Emery et al., 2009)	0–10	Pharmaceutical powders (API, Aspartame, HPMC, Respitose)/density meter, translational ST/HR, Carr index, AOR, FF	The effect of *RH* on the flow factor depends on particle shape. Increasing or decreasing flowability depends on the powder nature.
(Landi et al., 2011)	13–98	Glass beads/Schulze RST/YL	Cohesion and AIF increase only at high *RH*. Model linking bulk and particle scales.
(Landi et al., 2012)	0–70	Glass beads/Couette fluidized bed rheometer, Schulze RST/torque	Torque decreases with air velocity, and exhibits a non-monotonous trend with *RH*. The proposed rheological model is a function of flow properties.
(Karde et al., 2015)	30–90	Pharmaceutical powders: (Corn starch, Avicel PH 105, ibuprofen)/Freeman FT4 Powder Rheometer, Surface energy analyser/UYS, specific surface energy	Specific surface energy and flow behaviour are correlated. Hydrophilic powders are influenced by *RH*, in contrast to hydrophobic powders.
(Lumay et al., 2016)	0–95	Lactose/GranuDrum/Cohesive index	The cohesive index increases at very high *RH*.
(Lu et al., 2017)	0, 30, 58, 85	Lactose powders/Freeman FT4 powder rheometer/Flow energy	Flow energy increases with increasing relative humidity and fraction of fine particles.
(Karde et al., 2017)	30–90	Corn starch/Freeman FT4 powder rheometer/YL	Cohesion increases gradually with *RH* at low consolidation stress (<2 kPa), while it shows a minimum value for an intermediate value of *RH* at higher consolidation stress (3–9 kPa).
(Groen et al., 2020)	5–90	Coffee creamer, Citric acid monohydrate/Anton Paar powder rheometer/torque	Moderate increase of torque for $RH < 60$ %; for higher significant change of the slope. Temperature increase reduces the critical *RH* value.
(Salehi et al., 2021)	0–90	Mannitol powder/Brookfield powder flow tester, surface energy analyser/YL, FF, specific surface energy	Flowability remains unchanged for $RH < 60$ % with a temperature effect observed in the range 25–35 °C. A comparison of estimated interparticle forces is made using different theories (Rumpf model and a combination of the Kelvin model with the Laplace–Young equation).
(Marchetti et al., 2022)	40, 60, 80	Steel powder/Freeman FT4 powder rheometer/Flow energy, UYS	Flow energy and specific energy increase with *RH* beyond a critical value. Limited effect of *RH* on UYS.

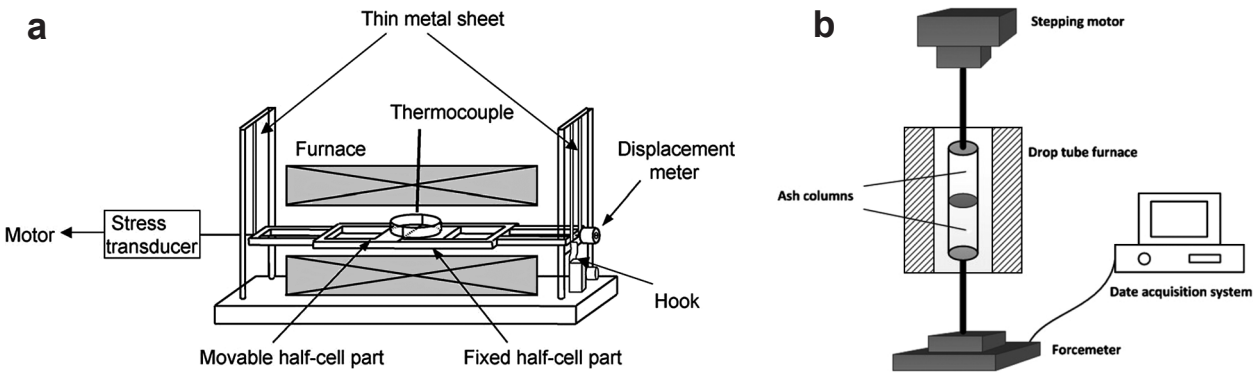

Fig. 8 **a)** Split-type tensile-strength testing system, reprinted with permission from Ref. (Kamiya et al., 2002b). Copyright: (2002) Elsevier; **b)** High-temperature solid bridge force device, reprinted with permission from Ref. (Luan and You, 2015). Copyright: (2015) Elsevier.

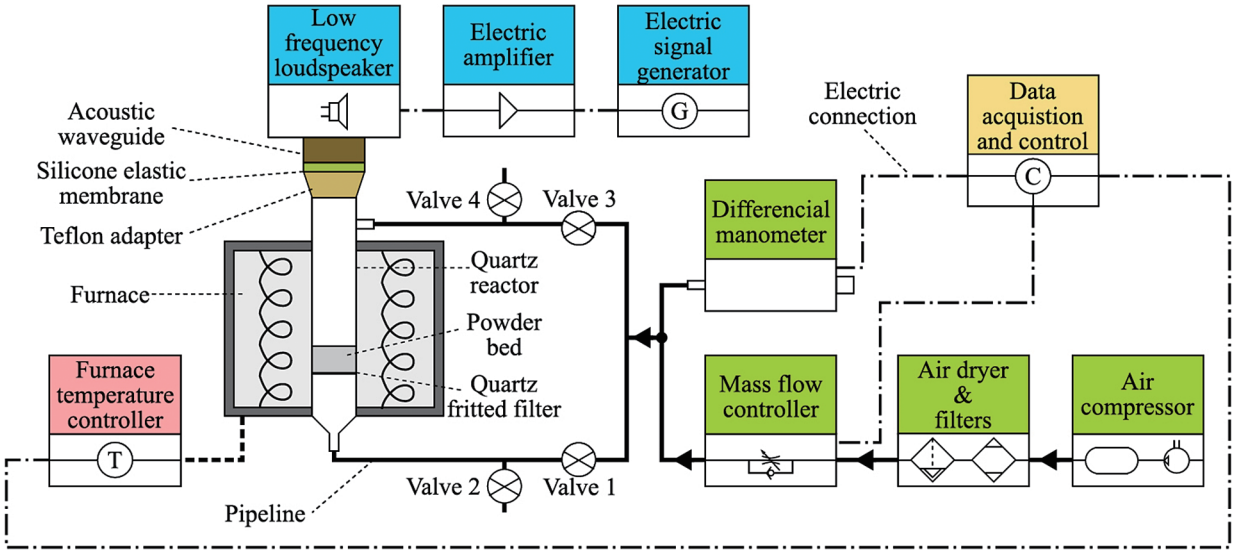

Fig. 9 Setup of the high-temperature Sevilla powder tester. Reprinted with permission from Ref. (Durán-Olivencia et al., 2020). Copyright: (2020) Elsevier.

specimen failure was measured.

The high-temperature Sevilla powder tester (HTSPT) is a modified version of the Sevilla Powder Tester that can reach temperatures up to 500 °C using a quartz fluidisation column surrounded by an electrical furnace (Durán-Olivencia et al., 2021; Espin et al., 2020) (**Fig. 9**). A low-frequency sound wave generation system was implemented on top of the powder bed to obtain the fluidisation state even with very cohesive powders. The tensile strength measurement was based on the measurement of the maximum pressure drop value during a fluidisation test at increasing gas velocity, as in the original apparatus for tests at ambient temperature. An initial preparation of the powder bed with a downward gas flow allowed consolidation of the sample under set values of resulting normal stress (Durán-Olivencia et al., 2020; Gannoun et al., 2022).

Tests were performed for various fly ashes derived from the combustion of coal and biomass particles (Horiguchi et al., 2018; Kamiya et al., 2002b; Liu et al., 2022; Tsukada et al., 2003, 2008) for mixes of silica coated with alkali metals (Kamiya et al., 2002a) and for calcium carbonate particles (Horiguchi et al., 2021b; 2022).

3.2.2 Shear testing experiments

First attempts at the conduction of shear experiments at high temperatures were performed using conventional shear cells heated before or during the test by placing a translational cell in an oven (Kanaoka et al., 2001; Smith et al., 1997) or in a muffle furnace (Maarup et al., 2014). Afterwards, the rheometers and shear cells were modified for conditions different from the ambient temperature. Zimmerlin et al. (2008) developed a rheometer based on a viscosimeter design to measure the torque necessary for the rotation of an impeller formed by a thin shaft with some orthogonal pins in a cylindrical cell heated by a coaxial furnace up to 700 °C. Ripp and Ripperger (2010) modified a Schulze annular shear cell to obtain temperatures lower and higher than ambient by introducing the flow of a heat transfer medium in a double casing of the though at the bottom of the ring cell (internal volume about 900 mL).

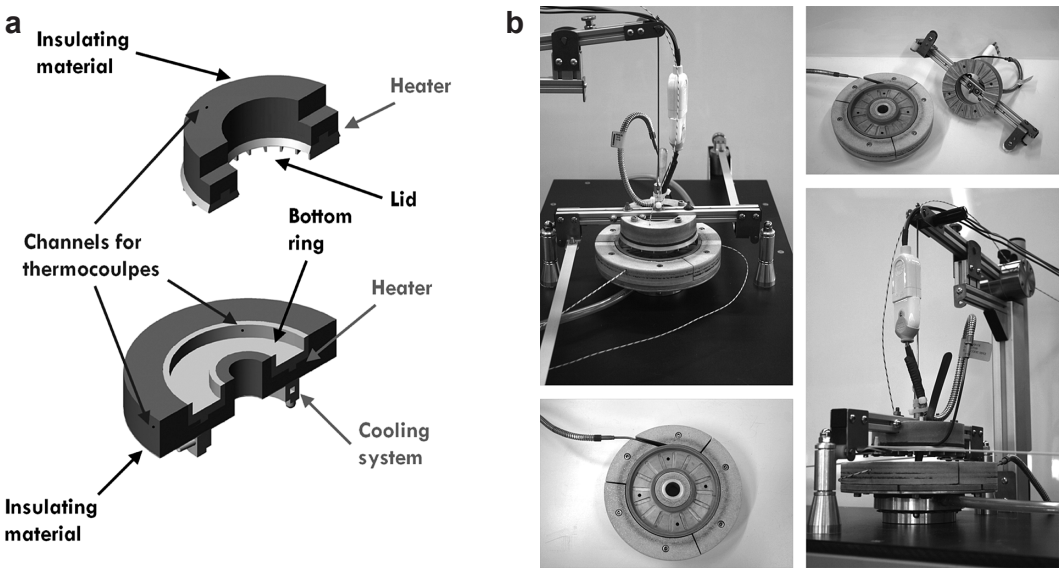

Fig. 10 High-temperature annular shear cell: **a)** cell and lid sketch; **b)** whole setup. Reprinted with permission from Ref. (Tomasetta et al., 2013). Copyright: (2013) Elsevier.

The setup was provided with conductive plates to achieve a uniform temperature distribution. The lid was provided with a thermal insulation layer for the cooling case and electric resistances for the heating case. Shear tests at temperatures between –80 °C and 120 °C were reported.

Tomasetta et al. (2013) developed a high-temperature annular shear cell (HT-ASC) (**Fig. 10**) by designing a ring bottom cell (internal volume of about 85 mL) and a lid electrically heated provided with a thermal insulation system consisting of a layer of ceramic material and a casing with flowing cooling water for the bottom cell in contact with a Schulze ring shear tester bench. Operating conditions allowed reaching temperatures from ambient to 500 °C.

More recently, a commercial shear cell with temperature and relative humidity control was developed by Anton Paar GmbH. It consists of an annular shear cell (internal volume: small cell 4.3 mL and large cell 18.9 mL) positioned in a heat transfer system based on combined convection and radiation to cover the temperature range from –160 °C to 600 °C (Barletta et al., 2019).

Investigations by shear testing at high temperatures have considered several powders with very different chemical natures, particle size distributions, and particle shapes, including fly ashes (Kanaoka et al., 2001; Liu et al., 2018), $MgSO_4$ and $CaSO_4$ powders (Smith et al., 1997), food powders (Ripp and Ripperger, 2010), ceramic powders (Chirone et al., 2016, 2018; Tomasetta et al., 2013), catalyst and catalyst support powders (Tomasetta et al., 2013; Zinatlou Ajabshir et al., 2022), titanium dioxide powders (Macrì et al., 2017b), and polymer powders for additive manufacturing (Ruggi et al., 2020a; 2020b).

In addition to measuring complete yield loci and flow functions according to the shear testing standards, a simplified experimental procedure for quicker scrutiny of the effect of temperature on flowability was proposed by Chirone et al. (2018). The shear stress was measured in the HT-ASC during a single sequence of pre-shear and shear steps under decreasing normal stress, as it is recommended to measure a single point for a static yield locus at increasing temperature values (**Fig. 11**). This protocol allowed the preliminary detection of critical temperature values for the change in interparticle forces. As a result, complete shear tests can be focussed on a narrower temperature interval to obtain the corresponding flow functions. Experimental results were generally reported in terms of yield loci and flow functions at consolidation stresses between 1 and 14 kPa, but more often at low consolidation stresses between 0.75 and 2 kPa, to reproduce the typical range of stresses experienced by the powders in process units such as fluidised beds

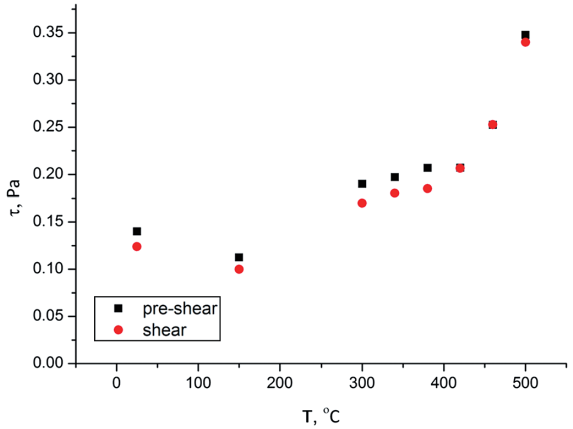

Fig. 11 Shear stress as a function of temperature for a ceramic powder with low-melting impurities. Reprinted with permission from Ref. (Chirone et al., 2018). Copyright: (2018) Elsevier.

(Chirone et al., 2020; Macrì et al., 2020) and selective laser sintering machines (Ruggi et al., 2020a; 2020b).

3.3 Effect of temperature on bulk flow properties in the presence of capillary forces

When powders are characterised by some moisture content at ambient temperature and are not melting at relatively low temperatures, the prevailing phenomena affecting flow properties are related to water evaporation. By increasing the temperature above 100 °C, capillary forces vanish, and the only active interactions remaining are van der Waals forces. At the bulk scale, these changes can be detected as a decrease in tensile strength, cohesion, and unconfined yield strength between ambient and temperatures just above 100 °C (Chirone et al., 2018; Ruggi et al., 2020a).

For higher temperatures or dry powders, a temperature increase is generally associated with an increase in cohesion and tensile strength, which can be related to either the rise of van der Waals forces or the eventual formation of a liquid phase. Given the high intensity of capillary forces, a melting phase is generally associated with a sharp increase in powder cohesion or tensile strength. Such phenomena have been observed in shear testing experiments with polymeric powders (Ruggi et al., 2020a; 2020b) or ceramic powder mixtures containing salt impurities (Chirone et al., 2018). It is remarkable that while for polymeric powders, DSC revealed that the increase in powder cohesion is related to the approach to the polymer melting temperature (Ruggi et al., 2020a; 2020b), for ceramic powder mixtures with salt impurities, neither DTA nor TGA could show the phase transition of low melting salts due to the minimal quantities of these salts present only on the particle surface. Such salt presence could be indirectly proven by EDX analysis and information on the reactive system to which the particles had been exposed. In this respect, the single-point pre-shear/shear analysis proposed above and reported in **Fig. 11** appeared to be more sensitive to phase changes limited to the particle surface than the established thermal analysis procedures (Chirone et al., 2018).

Similar phenomena linked to capillary forces were observed in tensile strength experiments on ash materials containing low melting compounds associated with the presence of eutectic oxides (Horiguchi et al., 2021b) or the addition of highly reacting calcium carbonate nanoparticles (Horiguchi et al., 2022). Proof of this interpretation is found in the similar behaviour found in artificial mixtures of silica particles coated with alkali metals, such as sodium and potassium (Kamiya et al., 2002a), or phosphorous (Horiguchi et al., 2021a). Care should be taken when using such a model system because it was also noted that when the interparticle liquid phase is formed by the fusion of low melting compounds, some evaporation due to the increasing temperature can occur and result in a slight decrease in the tensile strength (Tsukada et al., 2003).

Chirone et al. (2018) proved that the significant increase in the cohesive strength of ceramic powders at high temperatures (500 °C) was due to the rise of capillary forces using a model approach similar to that proposed by Pierrat and Caram (1997), assuming the partial melting of all salts present in the powder. The characteristic size of the contact area where the capillary bridge formed was estimated using the Rumpf model applied to the tensile strength value measured at low temperature for the dry powder, assuming the presence of van der Waals forces only.

In general, clear indications of a molten capillary phase come from the effects of system cooling, which may transform bridges from liquid to solid at interparticle contact surfaces. The result is a stronger bond between particles and, thus, a higher strength at the bulk level, as found in tensile testing experiments (Hurley and Dockter, 2003; Luan and You, 2015). Another coherent phenomenon is the observed shrinkage of the hot powder bed, which can be explained by the partial sintering of the particle surfaces in contact with the mobility of the molten phase (Kamyabi et al., 2017).

3.4 Effect of temperature on bulk flow properties in the presence of van der Waals forces

3.4.1 Theoretical background

The intensity of van der Waal forces tends to be a few orders of magnitude smaller than capillary forces (e.g. 10^{-8}, vs 10^{-6} N) and is more strongly dependent on the local contact geometry (Chirone et al., 2018), thus significantly changing from particle to particle. Perhaps, for this reason, no direct measurement of the effect of temperature on van der Waals forces is available, as reported in **Section 3.1** above.

Van der Waals forces, F_{vdW}, between spheres of radiuses r_1 and r_2 are well described by the following simple equation:

$$F_{vdWs} = \frac{A}{6a^2}\left(\frac{r_1 r_2}{r_1 + r_2}\right) = \frac{A}{12a^2} r \tag{13}$$

where A is the Hamaker constant, a is the shortest distance between the particle surfaces, and r represents the average radius. For contacting spheres $a = a_0 = 4 \cdot 10^{-10}$ m, the conventional distance is assumed between atomic layers in crystals (Israelachvili, 2011). The short-range characteristics of van der Waals interactions allow the extension of **Eqn. (13)** to the shapes of real particles, assuming for r_1 and r_2 the local curvature radius of the particle surfaces at the contact point. However, in real particles, the surface at the contact point can deform due to the attraction force, eventually combined with external compaction forces. A simplified but comprehensive approach in the presence of a consolidation force, F_N, was proposed by Tomas (Tomas, 2004), who proposed a simple static force balance between the contacting particles, assuming that the attractive van

der Waals force is obtained by simply summing the contributions of the van der Waals force between the undeformed particles and the attractive force, F_{vdWp}, developed by the area of the flattened surface at the contact point:

$$F_N + F_{vdWs} + F_{vdWp} = F_{el} + F_{pla} \tag{14}$$

where F_{el} and F_{pla} are the repulsive force components due to the contact's elastic and plastic deformation, respectively. In particular, assuming a circular footprint of the contact area of radius r_c, it is

$$F_{vdWp} = \pi r_c^2 \frac{A}{6a_0^3} \tag{15}$$

Eqn. (15) is derived from the general expression for van der Waals interactions between two planar surfaces. The complete calculations for F_{el} and F_{pla} were given by Tomas (Tomas, 2004) and depended on the material elasticity and the limiting yield strength of the particle surface. Under tensile conditions, the minimum force $F_P = -F_N$ necessary to separate the particle (pull-off) can be obtained from **Eqn. (14)** under conditions in which the contribution of the repulsive forces is nil:

$$F_P = F_{vdWs} + F_{vdWp} \tag{16}$$

In this situation, the flattened portion of the contact is limited to the portion permanently deformed during consolation. The F_{vdWp} and the r_c values at consolidation and pull-off coincide only for purely plastically deformable particles with an equal curvature radius at contact r. In this case, the Molerus equation (Molerus, 1975) is obtained as follows:

$$F_P = \frac{A}{12a_0^2} r \frac{1+(2F_N/\pi p_f r a_0)}{1-(A/6\pi p_f a_0^3)} \tag{17}$$

where p_f is the material yield strength in a confined situation, such as that in the contact region, which can be related to the material hardness. In the case of simple isometric particle shapes with relatively narrow and unimodal particle size distributions, a single contact point between neighbouring particles can be assumed, and the Rumpf equation can provide a reasonable relationship between interparticle forces and major principal stress or strength, as follows:

$$\sigma_1 = (1-\varepsilon)\frac{kF_N}{\pi d^2} \tag{18}$$

$$\sigma_t = (1-\varepsilon)\frac{kF_P}{\pi d^2} \tag{19}$$

The Hamaker constant is scarcely dependent on temperature changes within the proper ranges of chemical processes. Therefore, the effect of temperature on van der Waals forces is mostly related to changes in the material hardness with temperature. Lower material hardness corresponds to larger permanent deformations at the contacts, larger values of F_{vdWp} at pull-off, and larger material cohesion, both in the case of purely plastic deformation and elastic–plastic deformations of contacts.

3.4.2 Experiments qualitatively supporting the theory

Quantitative verification of the above-described theory requires knowledge of several physical parameters such as the geometry and number of binary particle contacts, effective material hardness and elasticity at the contact points and test temperature, and their distribution in the powder sample. Therefore, the theory can often be used only for qualitatively interpreting the observed results of experiments in which the effect of temperature on tensile strength or shear testing is measured. Experiments are limited to systems in which cohesion is dominated by van der Waals forces, i.e., for materials that do not exhibit any liquid formation, such as calcium carbonate and silicon carbide powders and soda-lime glass beads. In these systems, it has been verified that temperature changes significantly combine with consolidation and particle size to determine changes in the directly measured tensile strength (Durán-Olivencia et al., 2020, 2021; Espin et al., 2020). At a consolidation stress of 2 kPa, the tensile strength showed a much greater increase (up to ten times for $CaCO_3$) for $T > 300$ °C compared with that at very low consolidation (1 kPa) (Durán-Olivencia et al., 2020). Regression of experimental results over a range of temperatures between ambient and 500 °C and at a low range of consolidation stresses between 0.37 and 2 kPa allowed the derivation of different empirical correlations of the tensile strength as a function of temperature and consolidation stress (Durán-Olivencia et al., 2020; 2021). Considering powders of the same material and different mean particle sizes, the same order of magnitude percentage increase in the tensile strength was observed at lower temperatures (Espin et al., 2020) with smaller particle sizes. Increases of different magnitudes of the tensile strength for different materials were justified with a changing effect of temperature on the material hardness: the larger the hardness reduction, the more significant was the necessary pull-off force at the particle level and, therefore, the larger was the tensile strength at high temperature (Durán-Olivencia et al., 2021). The intensity of the temperature effect was also qualitatively correlated with the glass transition temperature and the Tamman temperature for glassy and non-glassy materials, respectively. For example, for soda lime glass beads, approaching the glass transition temperature, a significant hardness reduction could occur, and the surface particle could undergo some "softening" corresponding to a larger pulling force for particles in contact.

In shear testing experiments, elevated temperature mainly affected powder cohesion, whereas changes in the angle of internal friction were generally negligible. The

increase of cohesion with increasing temperature resulted in a vertical shift of the yield locus, corresponding to a rise in the unconfined yield strength f_c and of the extrapolated tensile strength σ_t, but to a much more limited extent in the major principal stress σ_1. Consequently, when a thermal effect was observed, the flow functions at higher temperatures shifted upward with respect to those at ambient temperature, and the flow factor σ_1/f_c values increased. The effect of voidage changes due to temperature appeared to be much less significant in affecting interparticle forces and, thus, cohesive powder strength.

For ceramic powders, catalyst powders, and glass beads without low melting components, the increase in the unconfined yield strength was between 50 % and 100 % (Chirone et al., 2016; Macrì et al., 2017b; Tomasetta et al., 2013). The highest increase values were recorded at higher consolidation stress (Tomasetta et al., 2013) and for finer particles. The corresponding growth of the flow factor could shift the flowability class of the powder, especially when the flow function at ambient temperature lies close to the borders of neighbouring classes. For instance, this happened to the fine-cut 20–38 μm of silicon powders, resulting in an easy-flowing classification at ambient temperature while becoming cohesive at 500 °C (Chirone et al., 2016). A more substantial change in class of flowability was observed for zeolites passing gradually, with increasing temperature, from free-flowing at 150 °C to easy-flowing at 300 °C and to cohesive behaviour at 500 °C (Zinatlou Ajabshir et al., 2022) (**Fig. 2**). Thermal analysis excluded the occurrence of any melting in the powder sample.

In the literature, different explanations than those given at the beginning of this section are provided to justify the observed changes in the measured flow properties with temperature. Tensile strength experiments on complex materials, such as ashes, were coupled with X-ray diffractometry, Fourier transform infrared analysis (FTIR), field emission scanning electron microscopy (FESEM), and thermomechanical characterisation to deeply investigate the chemical composition and particle morphology changes with temperature. According to Horiguchi et al. (2022; 2021b), the increase in van der Waals forces was mainly due to the thermal expansion of particles, which may cause an increase in the interparticle contact area and a reduction in the distance between particles. Moreover, in some cases, temperature could change the molecular characteristics (e.g. the amount of free silanol group on silica) on the surface of the particles, which affects the intensity of the van der Waals forces (Kamiya et al., 2002b).

On the other hand, the presence of several additives, such as diatomite microparticles (Tsukada et al., 2008), alumina nanoparticles (Horiguchi et al., 2018), iron oxide (Fe_3O_4) microparticles (Horiguchi et al., 2021a), and kaolin and vermiculite microparticles (Liu et al., 2022), was demonstrated to decrease the tensile strength of ashes due to the increase of interparticle porosity or to prevent the generation of eutectic compounds. These findings indicate that a strategic choice of additives to coal can reduce the increase in cohesive strength at high temperatures due to the formation of a liquid phase.

3.4.3 Experiments quantitatively supporting the theory

Tomasetta et al. (2014) showed that the assumption of plastic deformation of the interparticle contact area due to the local consolidation force, according to Molerus (1975), was necessary to correctly predict the change in cohesive strength with consolidation stress under dry conditions. Chirone et al. (2016) demonstrated that the temperature effect on the intensity of van der Waals forces mainly depends on the increase in the interparticle contact area, which is determined by a decrease in the yield strength of the particle material with increasing temperature. Similar conclusions were drawn by Macrì et al. (2017b), who replaced the Molerus model with the Tomas equations (Tomas, 2000) for the interparticle adhesive forces in the framework of the Rumpf approach, and by Macrì et al. (2017a), who applied the Tomas model relating flow factors and angles of internal friction, derived from the yield locus, directly to the elastic–plastic contact consolidation coefficient (Tomas, 2004). More recently, this interpretation was also confirmed by Espin et al. (2020), who derived the relationship between microscopic consolidation force and adhesion force from data on consolidation stress and tensile strength experimentally measured using HTSPT.

Zinatlou Ajabshir et al. (2022) highlighted the role of the presence of fines for a zeolite powder with a wide particle size distribution in the definition of a more or less significant effect of temperature on flowability. This finding was explained with the Rumpf model corrected to consider the effect of a bimodal distribution with micrometric-sized core host particles coated by smaller satellite or guest particles in the form of agglomerates. The satellite particles act as spacers between the core particles and define the actual geometry and distribution of the interparticle contacts. In particular, for these powders, a key role is played by the increased number of active contacts between two neighbouring agglomerates. Therefore, the more cohesive powder resulted in the one with smaller satellites, which ensured a higher number of active contacts between particles. Even if singularly taken at the satellite level, the consolidation forces and the cohesion forces are relatively small. Instead, the material with a more limited number of larger satellite particles in the agglomerate showed better flow properties for the limited number of contacts between adjacent agglomerates. However, both the contact force and consolidation forces calculated for the contact points between satellite particles were larger than those in the other powder and, likely, more affected by contact

Table 3 Overview of case studies on the effect of temperature on powder strength, friction, and cohesion (chronological order). (Continued on next page)

References	Temp. (°C)	Powders/Tester/Properties	Main results
(Smith et al., 1997)	22, 750	$CaSO_4$, $MgSO_4$, alone and mixtures/Jenike ST/FF	Increase in the UYS at higher temperatures.
(Kanaoka et al., 2001)	20–950	Coal fly ashes/Heated translational ST/YL	Increase in cohesion beyond a critical temperature value depending on the lime content in the ashes and on the gas component exposition (N_2 or CO_2) due to solid bridges (sintering).
(Kamiya et al., 2002b)	25–850	Silica and fly ashes/Heated split-cell TS tester/TS	Moderate increase of TS up to 1000 K, sharp increase at higher temperatures.
(Kamiya et al., 2002a)	25–850	Silica coated with alkali metals/Heated split-cell TS tester/TS	Melting of alkali metals causes a dramatic increase in TS for $T > 700$ °C.
(Hurley and Dockter, 2003)	700–750	Combustion gas filter dust/ Heated split-cell TS tester/TS	The ratio between TS and the density of the ashes cake on the hot gas filter is presented as a key parameter.
(Tsukada et al., 2003)	25–900	Biomass combustion ashes/ Heated split-cell TS tester/TS	TS increases from 400 to 700 °C due to liquid phase formation, while it decreases above 700 °C due to liquid evaporation.
(Hurley et al., 2006)	300–800	Combustion gas filter dust/ Heated split-cell TS tester/TS	TS increase depends on the temperature and pressure drop across the filter, acting as a consolidation stress. The higher strength increase is due to partial melting. Role of the reactions at intermediate temperatures.
(Tsukada et al., 2008)	20–600	Fly ashes with additives/ Heated split-cell TS tester/TS	Addition of 100 µm diatomite and silica sand particles reduces TS at $T > 700$ °C, while water-quenched molten slag particles with aluminium increase it.
(Zimmerlin et al., 2008)		Soda-lime glass, gypsum, sodium chloride, potassium chloride/High temperature rheometer/Torque	Torque increases above 400–450 °C. The component mixture reproduces the ashes' behaviour with temperature.
(Ripp and Ripperger, 2010)	–78–220	Polyester granulates, lactose, ground coffee, polyphosphates, cocoa powder, dry ice/ Modified Schulze RST/YL, FF	Different temperature effects depending on the material.
(Tomasetta et al., 2013)	25, 500	Fluid cracking catalysts, Fly ashes, Corundum, Synthetic α-alumina, Glass beads, Mix of glass beads and 1 % HDPE/HT-ASC/YL, FF	Very limited effect of temperature on flow properties, except for glass beads with 1 % HDPE exhibiting a significant increase in cohesion at 500 °C.
(Maarup et al., 2014)	22–850	Cement raw meal/Translational ST in a muffle/UYS	UYS increases above 550 °C.
(Luan et al., 2015)	750–1250	Ashes/High-temperature solid bridge force device (HTSBFD)/TS	Significant increase in TS above 1150 °C. TS is correlated with the solid bridge force.
(Shao et al., 2016)	25–800	Biomass combustion ashes/ Heated split-cell TS tester/TS	DEM model predictions compared with the experiments.
(Chirone et al., 2016)	25, 500	Ceramic powders/HT-ASC/ YL, FF	A simplified experimental procedure allows quicker preliminary detection of the critical temperature for flowability change. Temperature mainly affects cohesion, whereas the AIF results remain independent of temperature. A proposed model links interparticle forces to TS.
(Macrì et al., 2017a, b)	25, 500	Titanium dioxide synthetic rutile and natural rutile/ HT-ASC/YL, FF	More significant decrease in flowability at 500 °C for synthetic rutile. Proposed model linking interparticle forces to TS.

Table 3 Overview of case studies on the effect of temperature on powder strength, friction, and cohesion (chronological order). (Continued from previous page)

References	Temp. (°C)	Powders/Tester/Properties	Main results
(Chirone et al., 2018)	25, 500	Ceramic powders/HT-ASC/YL, FF	The presence of low-melting impurities determines a significant reduction in flowability with temperature. A proposed model aims to link capillary forces and TS.
(Horiguchi et al., 2018)	25–900	Fly ashes with alumina additives/Heated split-cell TS tester/TS	The addition of alumina nanoparticles reduces the increase in TS of ashes due to their positive effect on porosity and chemical composition.
(Liu et al., 2018)	25, 500	Fly ashes/HT-ASC/YL, FF	Moderate decrease in flowability at 500 °C. A proposed model links interparticle forces to TS considering PSD.
(Espin et al., 2020)	25–500	Limestone/HTSPT/TS	The increase in TS with temperature is more significant for finer powders.
(Ruggi et al., 2020a, b)	25–160	Polyamide 12 and 6/HT-ASC/YL, FF	Dramatic increase in UYS at temperatures approaching the melting point. The Bond number provides a qualitative correlation with spreading behaviour.
(Durán-Olivencia et al., 2020)	25–500	Calcium carbonate/HTSPT/TS	TS increases above 200 °C, and is more pronounced at consolidation stress > 1 kPa due to softening caused by hardness reduction.
(Durán-Olivencia et al., 2021)	25–500	Soda-lime glass beads, silicon carbide, limestone/HTSPT/TS	TS increases with temperature for all materials, emphasizing the temperature dependence of material hardness.
(Horiguchi et al., 2021a)	25–800	Synthetic ashes/Heated split-cell TS tester/TS	Phosphorus leads to a marked increase in the adhesiveness of synthetic ashes at temperatures > 600 °C, whereas the presence of Fe_3O_4 reduces the strength, withparticular relevance to ashes from incinerated sewage sludge.
(Horiguchi et al., 2021b)	25–500	Calcium carbonate, alumina, silica/Heated split-cell TS tester/TS	Temperature affects the TS of $CaCO_3$ at T > 500 °C, with negligible effect on alumina and silica microparticle. The addition of alumina to calcium carbonate hinders the temperature effect on strength.
(Horiguchi et al., 2022)	25–900	Silica, kaolin, calcium carbonate, alumina/Heated split-cell TS tester/TS	The addition of calcium carbonate nanoparticles to kaolin powder at 900 °C increases TS. However, this effect is not observed when added to silica powder. The presence of alumina in mixtures suppresses the strength increase with temperature.
(Liu et al., 2022)	800–1200	High calcium coal ash powders/High-temperature TS tester/TS	Tensile strength increases above 800 °C, with a steep rise at 1100 °C. Additives with a low-temperature eutectic enhance the ash TS.
(Zinatlou Ajabshir et al., 2022)	150, 300, 500	Zeolite/Anton Paar shear cell/YL, FF	Flowability decreases with temperature, and the more significant effect on one sample is theoretically explained by the different PSDs.

plasticisation, resulting in a larger temperature effect on the flowability of this material.

Macrì et al. (2017a) and Zinatlou Ajabshir et al. (2022) provided quantitative evidence that the most relevant material property related to the effect of temperature on the change in van der Waals interparticle forces is the hardness of the particle material.

Ruggi et al. (2020b) estimated the interparticle force for some polyamide powders used in additive manufacturing, exhibiting a change in flowability class from easy flowing to very cohesive when the temperature increased to values close to their melting point. These authors found that the ratio between the granular Bond number value close to the melting temperature and that at 100 °C under dry conditions was greater than 100.

Table 3 reports a detailed survey of the studies on the effect of temperature.

4. Conclusions and perspectives

Process conditions inducing the presence of liquid in the interparticle volume due to either liquid addition, partial melting of solids, or capillary condensation from a humid gas atmosphere give rise to capillary bridges and capillary forces. The intensity of the forces depends on the liquid

saturation level. The resulting cohesive strength of a powder, free flowing or easy flowing under dry conditions, can increase when liquid bridges are in the pendular regime until the achievement of a plateau value. Then, for the funicular regime, the strength continues to grow. Pendular and funicular regimes typically correspond to liquid contents between 1 % and 15 % or between 15 % and 40 %, respectively, assuming a specific gravity of approximately 1.5. Only in the capillary regime is a dramatic decrease in cohesive strength observed due to the dominant reduction of capillary pressure. Instead, for a powder exhibiting cohesion due to van der Waals forces, a limited amount of liquid can initially reduce the strength, but the previously described trend is recovered by further increasing the liquid content.

Temperature rise above 100 °C under atmospheric conditions can dry the moisture eventually present between particles in bulk. Vanishing of capillary forces makes the powder less cohesive because of the lower intensity of van der Waals forces. Further temperature rise can strengthen these interactions due to the enhancement of plastic deformation at interparticle contacts, especially for high consolidation stress due to reduced particle material hardness. The consequent flattening of the contact and increase of the contact area is the main cause of the rise in van der Waals forces and of the reduction of powder flowability, which in general is limited to a shift from one class to the adjacent one (e.g. from free flowing to easy flowing, from easy flowing to cohesive). Low melting components or thermally activated reactions generating a liquid phase can determine the onset of capillary forces at critical temperatures, dramatically affecting powder flowability, which can change from free-flowing to cohesive behaviour. The significant influence of liquid content, humidity, and temperature on interparticle forces and bulk flow properties can explain the change in powder behaviour in units with peculiar process conditions. In fact, it was possible to qualitatively relate the increase in cohesive flow properties at low consolidation and the fluidisation behaviour, in terms of minimum velocity for fluidisation and bed expansion, due to the higher temperature effect on van der Waals forces (Chirone et al., 2020; Macrì et al., 2020). A direct link between interparticle forces and fluidisation properties was also demonstrated for the effect of environmental relative humidity (LaMarche et al., 2016).

Although general phenomenology has been explained qualitatively and quantitatively for various materials and different process conditions, the variability in particle shape, material composition, physical state, and temperature change of all relevant material properties in real systems make it challenging to theoretically predict the effect of a liquid phase or temperature. In fact, this requires a detailed characterisation of the surface morphological properties of particles (i.e. roughness and asperities size), which can be affected by wide distributions in real samples of industrial processes. Moreover, theoretical equations linking microscale forces and macroscale stresses, such as the Rumpf equation, could be affected by a certain degree of uncertainty in the case of non-ideal particles. Developing a completely predictive model is even more challenging in the case of low-melting impurities or chemical reactions activated by heating. As a result, direct characterisation of the flow properties of powder samples under conditions reproducing those of process units appears to be the main method for quantitative purposes. In this respect, conditioning a powder sample by adding liquid or exposure to humid air before performing any type of flow property test (e.g. tensile tester or shear tester) requires particular care to obtain uniform and stable liquid distribution in the specimen. This latter issue might be overcome in the near future by the use of purposely generated and calibrated discrete element method (DEM) models. However, the right way to proceed would require dedicated studies that are yet to be conducted.

As widely discussed in this review, suitable testers with reliable temperature control are presently available in the academic community to directly measure flow properties at high temperatures. However, nowadays, only one commercial instrument is known to reach temperatures up to 600 °C. Other instruments will likely come in the future to address wider needs. In particular, it might be of great scientific and industrial interest because of the possibility of reaching temperatures around 1000 °C, which is typical of several thermal and solar applications.

Acknowledgments

Sina Zinatlou Ajabshir research grant and part of the research were supported by MATHEGRAM, a Marie Sklodowska-Curie Innovative training network MATHEGRAM funded through the People Programme (Marie Sklodowska-Curie Actions) of the European Union's Horizon 2020 Programme H2020 under REA grant agreement No. 813202.

Nomenclature

AIF	angle of internal friction
AOR	angle of repose
FF	flow function
HR	Hausner ratio
HT-ASC	high-temperature annular shear cell
HTSPT	high-temperature Sevilla powder tester
MPT	Micron powder tester
PSD	particle size distribution
RST	ring shear tester
ST	shear tester
TS	tensile strength
UYS	unconfined yield strength
YL	yield loci
a	closest distance between particles (m)
A	Hamaker constant (J)

a'	constant in **Eqn. (6)** (-)
a_0	minimum distance at contact (m)
c	cohesion (Pa)
d	mean particle size (m)
f_c	unconfined yield strength (Pa)
F_c	capillary force (N)
F_{el}	elastic deformation repulsion force (N)
F_N	contact consolidation force (N)
F_p	pressure force (N)
F_{pla}	plastic deformation repulsion force (N)
F_s	surface tension force (N)
F_{vdWp}	van der Waals force for a flat surface (N)
F_{vdWs}	van der Waals force for a sphere or spherical contact (N)
ff_c	flow factor (-)
k	coordination number (-)
K	constant in **Eqn. (9)** (-)
M_W	molecular weight of water (kg/mol)
P_c	capillary pressure (Pa)
p_f	material hardness (Pa)
p_s	vapour pressure over a curved surface (Pa)
p_{s0}	vapour pressure of the liquid (Pa)
r	characteristic curvature radius of the particle surface at contact (m)
r_1; r_2	radii of particles 1 and 2 (m)
R_1	liquid bridge convex curvature radius (m)
R_2	liquid bridge concave curvature radius (m)
r_c	radius of the flattened surface at contact (m)
R_g	universal gas constant (J K^{-1} mol^{-1})
RH	relative humidity (-)
S	liquid saturation (-)
S_1	critical liquid saturation between the pendular and funicular states (-)
S_2	critical liquid saturation between the funicular and capillary states (-)
T	temperature (K)
x_w	liquid content by mass on a dry basis (-)
γ	liquid surface tension (N/m)
δ_0	characteristic roughness (m)
ε	powder bed voidage (-)
θ	liquid bridge contact angle (deg)
Δp	pressure difference between air and liquid (Pa)
ρ_l	liquid density (kg/m^3)
ρ_s	particle density (kg/m^3)
σ	normal stress (Pa)
σ_1	major principal stress (Pa)
σ_2	minor principal stress (Pa)
σ_t	tensile strength (Pa)
σ_{tc}	tensile strength in the capillary regime (Pa)
σ_{tp}	tensile strength in the pendular regime (Pa)
τ	shear stress (Pa)
ϕ	static angle of internal friction (deg)

References

Althaus T.O., Windhab E.J., Characterization of wet powder flowability by shear cell measurements and compaction curves, Powder Technology, 215–216 (2012) 59–65. https://doi.org/10.1016/j.powtec.2011.09.007

Althaus T.O., Windhab E.J., Scheuble N., Effect of pendular liquid bridges on the flow behavior of wet powders, Powder Technology, 217 (2012) 599–606. https://doi.org/10.1016/j.powtec.2011.11.026

Badetti M., Fall A., Hautemayou D., Chevoir F., Aimedieu P., Rodts S., Roux J.-N., Rheology and microstructure of unsaturated wet granular materials: experiments and simulations, Journal of Rheology, 62 (2018) 1175–1186. https://doi.org/10.1122/1.5026979

Barletta D., Poletto M., Santomaso A.C., Chapter 4. bulk powder flow characterisation techniques, in: Hare C., Hassanpour A., Pasha M. (Eds.), Powder Flow, Royal Society of Chemistry, Cambridge, UK, 2019, pp. 64–146, ISBN: 978-1-78801-224-9. https://doi.org/10.1039/9781788016100-00064

Bocquet L., Charlaix E., Ciliberto S., Crassous J., Moisture-induced ageing in granular media and the kinetics of capillary condensation, Nature, 396 (1998) 735–737. https://doi.org/10.1038/25492

Butt H.J., Capillary forces: influence of roughness and heterogeneity, Langmuir, 24 (2008) 4715–4721. https://doi.org/10.1021/la703640f

Butt H.-J., Kappl M., Normal capillary forces, Advances in Colloid and Interface Science, 146 (2009) 48–60. https://doi.org/10.1016/j.cis.2008.10.002

Capece M., Ho R., Strong J., Gao P., Prediction of powder flow performance using a multi-component granular Bond number, Powder Technology, 286 (2015) 561–571. https://doi.org/10.1016/j.powtec.2015.08.031

Capece M., Silva K.R., Sunkara D., Strong J., Gao P., On the relationship of inter-particle cohesiveness and bulk powder behavior: flowability of pharmaceutical powders, International Journal of Pharmaceutics, 511 (2016) 178–189. https://doi.org/10.1016/j.ijpharm.2016.06.059

Castellanos A., The relationship between attractive interparticle forces and bulk behaviour in dry and uncharged fine powders, Advances in Physics, 54 (2005) 263–376. https://doi.org/10.1080/17461390500402657

Chen W., Roberts A.W., A modified flowability classification model for moist and cohesive bulk solids, Powder Technology, 325 (2018) 639–650. https://doi.org/10.1016/j.powtec.2017.11.054

Chirone R., Barletta D., Lettieri P., Poletto M., Bulk flow properties of sieved samples of a ceramic powder at ambient and high temperature, Powder Technology, 288 (2016) 379–387. https://doi.org/10.1016/j.powtec.2015.11.040

Chirone R., Barletta D., Poletto M., Lettieri P., Detection and estimation of capillary interparticle forces in the material of a fluidized bed reactor at high temperature by powder flow characterization, Powder Technology, 330 (2018) 371–385. https://doi.org/10.1016/j.powtec.2018.02.024

Chirone R., Poletto M., Barletta D., Lettieri P., The effect of temperature on the minimum fluidization conditions of industrial cohesive particles, Powder Technology, 362 (2020) 307–322. https://doi.org/10.1016/j.powtec.2019.11.102

Coelho M.C., Harnby N., Moisture bonding in powders, Powder Technology, 20 (1978a) 201–205. https://doi.org/10.1016/0032-5910(78)80049-7

Coelho M.C., Harnby N., The effect of humidity on the form of water retention in a powder, Powder Technology, 20 (1978b) 197–200. https://doi.org/10.1016/0032-5910(78)80048-5

Cordova L., Bor T., de Smit M., Campos M., Tinga T., Measuring the spreadability of pre-treated and moisturized powders for laser powder bed fusion, Additive Manufacturing, 32 (2020) 101082. https://doi.org/10.1016/j.addma.2020.101082

Coughlin R.., Elbirli B., Vergara-Edwards L., Interparticle force conferred by capillary-condensed liquid at contact points, Journal of Colloid and Interface Science, 87 (1982) 18–30. https://doi.org/10.1016/0021-9797(82)90368-X

Durán-Olivencia F.J., Ebri J.M.P., Espín M.J., Valverde J.M., The cohesive behavior of granular solids at high temperature in solar energy storage, Energy Conversion and Management, 240 (2021) 114217. https://doi.org/10.1016/j.enconman.2021.114217

Durán-Olivencia F.J., Espín M.J., Valverde J.M., Cross effect between temperature and consolidation on the flow behavior of granular materials in thermal energy storage systems, Powder Technology, 363 (2020) 135–145. https://doi.org/10.1016/j.powtec.2019.11.125

Durán-Olivencia F.J., Gannoun R., Pérez A.T., Valverde J.M., Efficacy of nanosilica coatings in calcium looping reactors, Industrial & Engineering Chemistry Research, 62 (2023) 1373–1389. https://doi.org/10.1021/acs.iecr.2c03490

Eaves T., Jones T.M., Effect of moisture on tensile strength of bulk solids i: sodium chloride and effect of particle size, Journal of

Pharmaceutical Sciences, 61 (1972a) 256–261. https://doi.org/10.1002/jps.2600610226
Eaves T., Jones T.M., Effect of moisture on tensile strength of bulk solids ii: fine particle-size materials with varying inherent coherence, Journal of Pharmaceutical Sciences, 61 (1972b) 342–348. https://doi.org/10.1002/jps.2600610304
Elbirli B., Vergara-Edwards L., Coughlin R.W., Interparticle force conferred by capillary-condensed liquid at contact points, Journal of Colloid and Interface Science, 87 (1982) 31–45. https://doi.org/10.1016/0021-9797(82)90369-1
Emery E., Oliver J., Pugsley T., Sharma J., Zhou J., Flowability of moist pharmaceutical powders, Powder Technology, 189 (2009) 409–415. https://doi.org/10.1016/j.powtec.2008.06.017
Espin M.J., Duran-Olivencia F.J., Valverde J.M., Role of particle size on the cohesive behavior of limestone powders at high temperature, Chemical Engineering Journal, 391 (2020) 123520. https://doi.org/10.1016/j.cej.2019.123520
Francia V., Ait Ali Yahia L., Ocone R., Ozel A., From quasi-static to intermediate regimes in shear cell devices: theory and characterisation, KONA Powder and Particle Journal, 38 (2021) 3–25. https://doi.org/10.14356/kona.2021018
Gannoun R., Ebrí J.M.P., Pérez A.T., Valverde J.M., The Sevilla powder tester: a tool for measuring the flow properties of cohesive powders at high temperatures, KONA Powder and Particle Journal, 39 (2022) 29–44. https://doi.org/10.14356/kona.2022008
Ghadiri M., Pasha Mehrdad, Nan W., Hare C., Vivacqua V., Zafar U., Nezamabadi S., Lopez A., Pasha Massih, Nadimi S., Cohesive powder flow: trends and challenges in characterisation and analysis, KONA Powder and Particle Journal, 37 (2020) 3–18. https://doi.org/10.14356/kona.2020018
Groen J.C., Kooijman W., van Belzen D., Meesters G.M.H., Schütz D., Aschl T., Verolme P., Real-time in-situ rheological assessment of sticky point temperature and humidity of powdered products, KONA Powder and Particle Journal, 37 (2020) 176–186. https://doi.org/10.14356/kona.2020006
Gyulai A., Bauer W., Ehrenberg H., Dry electrode manufacturing in a calender: the role of powder premixing for electrode quality and electrochemical performance, ACS Applied Energy Materials, 6 (2023) 5122–5134. https://doi.org/10.1021/acsaem.2c03755
Haider C.I., Althaus T., Niederreiter G., Hounslow M.J., Palzer S., Salman A.D., A micromanipulation particle tester for agglomeration contact mechanism studies in a controlled environment, Measurement Science and Technology, 23 (2012) 105904. https://doi.org/10.1088/0957-0233/23/10/105904
Harnby N., Hawkins A.E., Vandame D., The use of bulk density determination as a means of typifying the flow characteristics of loosely compacted powders under conditions of variable relative humidity, Chemical Engineering Science, 42 (1987) 879–888. https://doi.org/10.1016/0009-2509(87)80046-5
Horiguchi G., Fujii R., Yamauchi Y., Okabe H., Tsukada M., Okada Y., Kamiya H., Toward stable operation of coal combustion plants: the use of alumina nanoparticles to prevent adhesion of fly ash, Energy & Fuels, 32 (2018) 13015–13020. https://doi.org/10.1021/acs.energyfuels.8b03043
Horiguchi G., Fujimoto T., Yoshinaga K., Okada Y., Kamiya H., Particle adhesion induced by calcium carbonate nanoparticles at 900 °C, Powder Technology, 405 (2022) 117514. https://doi.org/10.1016/j.powtec.2022.117514
Horiguchi G., Ito M., Ito A., Kamiya H., Okada Y., Role of phosphorus and iron in particle adhesiveness at high temperatures using synthetic ashes, ACS Sustainable Chemistry & Engineering, 9 (2021a) 15315–15321. https://doi.org/10.1021/acssuschemeng.1c05676
Horiguchi G., Kamiya H., García-Triñanes P., Evaluation and control of the adhesiveness of cohesive calcium carbonate particles at high temperatures, Advanced Powder Technology, 32 (2021b) 283–289. https://doi.org/10.1016/j.apt.2020.12.009
Hurley J.P., Dockter B.A., Factors affecting the tensile strength of hot-gas filter dust cakes, Advanced Powder Technology, 14 (2003) 695–705. https://doi.org/10.1163/15685520360731981
Hurley J.P., Mukherjee B., Mann M.D., Assessment of filter dust characteristics that cause filter failure during hot-gas filtration, Energy & Fuels, 20 (2006) 1629–1638. https://doi.org/10.1021/ef050303k
Israelachvili J.N., Intermolecular and Surface Forces, third edition, Academic Press, 2011, ISBN: 978-0-12-375182-9. https://doi.org/10.1016/C2009-0-21560-1
Jallo L.J., Ghoroi C., Gurumurthy L., Patel U., Davé R.N., Improvement of flow and bulk density of pharmaceutical powders using surface modification, International Journal of Pharmaceutics, 423 (2012) 213–225. https://doi.org/10.1016/j.ijpharm.2011.12.012
Jenike A.W., Storage and flow of solids, Bulletin No. 123, Bulletin of the University of Utah, 53 (1964) 56–56. <https://digital.library.unt.edu/ark:/67531/metadc1067072/> accessed28122023.
Johanson K., Rabinovich Y., Moudgil B., Breece K., Taylor H., Relationship between particle scale capillary forces and bulk unconfined yield strength, Powder Technology, 138 (2003) 13–17. https://doi.org/10.1016/j.powtec.2003.08.037
Kamiya H., Kimura A., Tsukada M., Naito M., Analysis of the high-temperature cohesion behavior of ash particles using pure silica powders coated with alkali metals, Energy & Fuels, 16 (2002a) 457–461. https://doi.org/10.1021/ef0102081
Kamiya H., Kimura A., Yokoyama T., Naito M., Jimbo G., Development of a split-type tensile-strength tester and analysis of mechanism of increase of adhesion behavior of inorganic fine powder bed at high-temperature conditions, Powder Technology, 127 (2002b) 239–245. https://doi.org/10.1016/S0032-5910(02)00117-1
Kamyabi M., Sotudeh-Gharebagh R., Zarghami R., Saleh K., Principles of viscous sintering in amorphous powders: a critical review, Chemical Engineering Research and Design, 125 (2017) 328–347. https://doi.org/10.1016/j.cherd.2017.06.009
Kanaoka C., Hata M., Makino H., Measurement of adhesive force of coal flyash particles at high temperatures and different gas compositions, Powder Technology, 118 (2001) 107–112. https://doi.org/10.1016/S0032-5910(01)00300-x
Karde V., Dixit D., Ghoroi C., Adhesion force approximation at varying consolidation stresses for fine powder under humid conditions, Advanced Powder Technology, 28 (2017) 346–355. https://doi.org/10.1016/j.apt.2016.09.023
Karde V., Ghoroi C., Fine powder flow under humid environmental conditions from the perspective of surface energy, International Journal of Pharmaceutics, 485 (2015) 192–201. https://doi.org/10.1016/j.ijpharm.2015.03.021
Kartik S., Balsora H.K., Sharma M., Saptoro A., Jain R.K., Joshi J.B., Sharma A., Valorization of plastic wastes for production of fuels and value-added chemicals through pyrolysis – a review, Thermal Science and Engineering Progress, 32 (2022) 101316. https://doi.org/10.1016/j.tsep.2022.101316
Kohonen M.M., Geromichalos D., Scheel M., Schier C., Herminghaus S., On capillary bridges in wet granular materials, Physica A: Statistical Mechanics and its Applications, 339 (2004) 7–15. https://doi.org/10.1016/j.physa.2004.03.047
LaMarche C.Q., Miller A.W., Liu P., Hrenya C.M., Linking micro-scale predictions of capillary forces to macro-scale fluidization experiments in humid environments, AIChE Journal, 62 (2016) 3585–3597. https://doi.org/10.1002/aic.15281
Landi G., Barletta D., Lettieri P., Poletto M., Flow properties of moisturized powders in a Couette fluidized bed rheometer, International Journal of Chemical Reactor Engineering, 10 (2012) A28. https://doi.org/10.1515/1542-6580.2993
Landi G., Barletta D., Poletto M., Modelling and experiments on the effect of air humidity on the flow properties of glass powders, Powder Technology, 207 (2011) 437–443. https://doi.org/10.1016/j.powtec.2010.11.033
Liu Y., Lu H., Barletta D., Poletto M., Guo X., Gong X., Jin Y., Bulk flow properties of fly ashes at ambient and high temperature, Particuology, 38 (2018) 113–125. https://doi.org/10.1016/j.partic.2017.04.013
Liu Z., Jin J., Zheng L., Zhang R., Wang Y., He X., Kong S., Zhai Z., Controlling the ash adhesion strength of Zhundong high-calcium coal by additives at high temperature, Fuel, 323 (2022) 124342. https://doi.org/10.1016/j.fuel.2022.124342
Louati H., Oulahna D., de Ryck A., Effect of the particle size and the

liquid content on the shear behaviour of wet granular material, Powder Technology, 315 (2017) 398–409. https://doi.org/10.1016/j.powtec.2017.04.030

Lu H., Guo X., Jin Y., Gong X., Effect of moisture on flowability of pulverized coal, Chemical Engineering Research and Design, 133 (2018) 326–334. https://doi.org/10.1016/j.cherd.2018.03.023

Lu X.-Y., Chen L., Wu C.-Y., Chan H.-K., Freeman T., The effects of relative humidity on the flowability and dispersion performance of lactose mixtures, Materials, 10 (2017) 592. https://doi.org/10.3390/ma10060592

Luan C., You C., A novel experimental investigation into sintered neck tensile strength of ash at high temperatures, Powder Technology, 269 (2015) 379–384. https://doi.org/10.1016/j.powtec.2014.09.031

Lumay G., Traina K., Boschini F., Delaval V., Rescaglio A., Cloots R., Vandewalle N., Effect of relative air humidity on the flowability of lactose powders, Journal of Drug Delivery Science and Technology, 35 (2016) 207–212. https://doi.org/10.1016/j.jddst.2016.04.007

Maarup C., Hjuler K., Dam-Johansen K., High temperature cement raw meal flowability, Powder Technology, 253 (2014) 686–690. https://doi.org/10.1016/j.powtec.2013.12.040

Macrì D., Barletta D., Lettieri P., Poletto M., Experimental and theoretical analysis of TiO_2 powders flow properties at ambient and high temperatures, Chemical Engineering Science, 167 (2017a) 172–190. https://doi.org/10.1016/j.ces.2017.03.057

Macrì D., Poletto M., Barletta D., Lettieri P., An investigation of the flow properties of rutile particles: fluidization behaviour linked with shearing studies, Powder Technology, 374 (2020) 544–559. https://doi.org/10.1016/j.powtec.2020.07.082

Macrì D., Poletto M., Barletta D., Sutcliffe S., Lettieri P., Analysis of industrial reactive powders flow properties at high temperature, Powder Technology, 316 (2017b) 131–138. https://doi.org/10.1016/j.powtec.2016.10.064

Marchetti L., Mellin P., Neil Hulme C., Negative impact of humidity on the flowability of steel powders, Particulate Science and Technology, 40 (2022) 722–736. https://doi.org/10.1080/02726351.2021.1995091

Molerus O., Theory of yield of cohesive powders, Powder Technology, 12 (1975) 259–275. https://doi.org/10.1016/0032-5910(75)85025-X

Mort P., Michaels J.N., Behringer R.P., Campbell C.S., Kondic L., Kheiripour Langroudi M., Shattuck M., Tang J., Tardos G.I., Wassgren C., Dense granular flow—a collaborative study, Powder Technology, 284 (2015) 571–584. https://doi.org/10.1016/J.POWTEC.2015.06.006

Orband J.L.R., Geldart D., Direct measurement of powder cohesion using a torsional device, Powder Technology, 92 (1997) 25–33. https://doi.org/10.1016/S0032-5910(97)03212-9

Pagliai P., Simons S.J.R., Rhodes D., Towards a fundamental understanding of defluidisation at high temperatures: a micro-mechanistic approach, Powder Technology, 148 (2004) 106–112. https://doi.org/10.1016/j.powtec.2004.09.004

Pierrat P., Agrawal D.K., Caram H.S., Effect of moisture on the yield locus of granular materials: theory of shift, Powder Technology, 99 (1998) 220–227. https://doi.org/10.1016/S0032-5910(98)00111-9

Pierrat P., Caram H.S., Tensile strength of wet granular materials, Powder Technology, 91 (1997a) 83–93. https://doi.org/10.1016/S0032-5910(96)03179-8

Pierrat P., Caram H.S., Tensile strength of wet granula materials, Powder Technology, 91 (1997b) 83–93. https://doi.org/10.1016/S0032-5910(96)03179-8

Pietsch W., Hoffman E., Rumpf H., Tensile strength of moist agglomerates, Industrial & Engineering Chemistry Product Research & Development, 8 (1969) 58–62. https://doi.org/10.1021/i360029a009

Pietsch W., Rumpf H., Haftkraft, kapillardruck, flüssigkeitsvolumen und grenzwinkel einer flüssigkeitsbrücke zwischen zwei kugeln, Chemie Ingenieur Technik, 39 (1967) 885–893. https://doi.org/10.1002/cite.330391502

Pietsch W.B., Tensile strength of granular materials, Nature, 217 (1968) 736–737. https://doi.org/10.1038/217736a0

Price R., Young P.M., Edge S., Staniforth J.N., The influence of relative humidity on particulate interactions in carrier-based dry powder inhaler formulations, International Journal of Pharmaceutics, 246 (2002) 47–59. https://doi.org/10.1016/S0378-5173(02)00359-9

Rabinovich Y.I., Adler J.J., Ata A., Singh R.K., Moudgil B.M., Adhesion between nanoscale rough surfaces: ii. measurement and comparison with theory, Journal of Colloid and Interface Science, 232 (2000a) 17–24. https://doi.org/10.1006/jcis.2000.7168

Rabinovich Y.I., Adler J.J., Ata A., Singh R.K., Moudgil B.M., Adhesion between nanoscale rough surfaces: i. role of asperity geometry, Journal of Colloid and Interface Science, 232 (2000b) 10–16. https://doi.org/10.1006/jcis.2000.7167

Rabinovich Y.I., Adler J.J., Esayanur M.S., Ata A., Singh R.K., Moudgil B.M., Capillary forces between surfaces with nanoscale roughness, Advances in Colloid and Interface Science, 96 (2002) 213–230. https://doi.org/10.1016/S0001-8686(01)00082-3

Richefeu V., El Youssoufi M.S., Radjaï F., Shear strength properties of wet granular materials, Physical Review E, 73 (2006) 051304. https://doi.org/10.1103/PhysRevE.73.051304

Ripp M., Ripperger S., Influence of temperature on the flow properties of bulk solids, Chemical Engineering Science, 65 (2010) 4007–4013. https://doi.org/10.1016/j.ces.2010.03.046

Ruggi D., Barrès C., Charmeau J.-Y., Fulchiron R., Barletta D., Poletto M., A quantitative approach to assess high temperature flow properties of a PA 12 powder for laser sintering, Additive Manufacturing, 33 (2020a) 101143. https://doi.org/10.1016/j.addma.2020.101143

Ruggi D., Lupo M., Sofia D., Barrès C., Barletta D., Poletto M., Flow properties of polymeric powders for selective laser sintering, Powder Technology, 370 (2020b) 288–297. https://doi.org/10.1016/j.powtec.2020.05.069

Rumpf H., The strength of granules and agglomerates, in: Knepper W.A. (ed.), Agglomeration, Wiley, New York, 1962, pp. 379–418.

Salehi H., Karde V., Hajmohammadi H., Dissanayake S., Larsson S.H., Heng J.Y.Y., Bradley M., Understanding flow properties of mannitol powder at a range of temperature and humidity, International Journal of Pharmaceutics, 596 (2021) 120244. https://doi.org/10.1016/j.ijpharm.2021.120244

Schubert H., Capillary forces - modeling and application in particulate technology, Powder Technology, 37 (1984) 105–116. https://doi.org/10.1016/0032-5910(84)80010-8

Schubert H., Herrmann W., Rumpf H., Deformation behaviour of agglomerates under tensile stress, Powder Technology, 11 (1975) 121–131. https://doi.org/10.1016/0032-5910(75)80037-4

Seville J., Tüzün U., Clift R., Processing of Particulate Solids, Springer Netherlands, Dordrecht, 1997, ISBN: 9780751403763. https://doi.org/10.1007/978-94-009-1459-9

Shao Y., Aoki N., Tong Z., Zhong W., Yu A., Kamiya H., Numerical and experimental study of tensile stresses of biomass combustion ash with temperature variation, Advanced Powder Technology, 27 (2016) 215–222. https://doi.org/10.1016/j.apt.2015.12.007

Smith D.H., Haddad G.J., Ferer M., Shear Strengths of heated and unheated mixtures of $MgSO_4$ and $CaSO_4$ powders. Model pressurized fluidized bed combustion filter cakes, Energy & Fuels, 11 (1997) 1006–1011. https://doi.org/10.1021/ef970037d

Sofia D., Chirone R., Lettieri P., Barletta D., Poletto M., Selective laser sintering of ceramic powders with bimodal particle size distribution, Chemical Engineering Research and Design, 136 (2018) 536–547. https://doi.org/10.1016/j.cherd.2018.06.008

Stevens N., Tedeschi S., Powers K., Moudgil B., El-Shall H., Controlling unconfined yield strength in a humid environment through surface modification of powders, Powder Technology, 191 (2009) 170–175. https://doi.org/10.1016/j.powtec.2008.10.001

Teunou E., Fitzpatrick J.., Effect of relative humidity and temperature on food powder flowability, Journal of Food Engineering, 42 (1999) 109–116. https://doi.org/10.1016/S0260-8774(99)00087-4

Tomas J., Particle adhesion fundamentals and bulk powder consolidation, KONA Powder and Particle Journal, 18 (2000) 157–169. https://doi.org/10.14356/kona.2000022

Tomas J., Mechanics of nanoparticle adhesion—A continuum approach, in: Mittal K.L. (ed.), Particles on Surfaces: Detection, Adhesion and Removal, Volume 8, 1st edition, CRC Press, 2003, pp. 183–229, ISBN: 9780429088131. https://doi.org/10.1201/9789047403333

Tomas J., Fundamentals of cohesive powder consolidation and flow, Granular Matter, 6 (2004) 75–86. https://doi.org/10.1007/s10035-004-0167-9

Tomas J., Schubert H., Fliessverhalten von feuchten Schüttgütern, Aufbereitungs-Technik, 26 (1985) 399–404.

Tomasetta I., Barletta D., Poletto M., The high temperature annular shear cell: a modified ring shear tester to measure the flow properties of powders at high temperature, Advanced Powder Technology, 24 (2013) 609–617. https://doi.org/10.1016/j.apt.2012.11.007

Tomasetta I., Barletta D., Poletto M., Correlation of powder flow properties to interparticle interactions at ambient and high temperatures, Particuology, 12 (2014) 90–99. https://doi.org/10.1016/j.partic.2013.02.002

Tregambi C., Troiano M., Montagnaro F., Solimene R., Salatino P., Fluidized beds for concentrated solar thermal technologies—a review, Frontiers in Energy Research, 9 (2021). https://doi.org/10.3389/fenrg.2021.618421

Tsukada M., Kawashima K., Yamada H., Yao Y., Kamiya H., Analysis of adhesion behavior of waste combustion ash at high temperatures and its control by the addition of coarse particles, Powder Technology, 180 (2008) 259–264. https://doi.org/10.1016/j.powtec.2007.04.005

Tsukada M., Yamada H., Kamiya H., Analysis of biomass combustion ash behavior at elevated temperatures, Advanced Powder Technology, 14 (2003) 707–717. https://doi.org/10.1163/15685520360731990

Weigert T., Ripperger S., Calculation of the liquid bridge volume and bulk saturation from the half-filling angle, Particle & Particle Systems Characterization, 16 (1999) 238–242. https://doi.org/10.1002/(SICI)1521-4117(199910)16:5<238::AID-PPSC238>3.0.CO;2-E

Zafar U., Vivacqua V., Calvert G., Ghadiri M., Cleaver J.A.S., A review of bulk powder caking, Powder Technology, 313 (2017) 389–401. https://doi.org/10.1016/j.powtec.2017.02.024

Zimmerlin B., Leibold H., Seifert H., Evaluation of the temperature-dependent adhesion characteristics of fly ashes with a HT-rheometer, Powder Technology, 180 (2008) 17–20. https://doi.org/10.1016/j.powtec.2007.03.014

Zinatlou Ajabshir S., Gucuyener C., Vivacqua V., Gobby D., Stitt H., Barletta D., Poletto M., Flow behaviour of zeolite powders at high process temperatures, Powder Technology, 409 (2022) 117818. https://doi.org/10.1016/j.powtec.2022.117818

Authors' Short Biographies

Dr. Sina Zinatlou Ajabshir is currently a Postdoctoral Fellow at the Department of Industrial Engineering of the University of Salerno (UNISA), working on powder properties for powder-based Laser 3D printing. He earned his BSc and MSc in materials science and engineering from the University of Tabriz and Sharif University of Technology (SUT), respectively. He completed his Ph.D. in Industrial Engineering with a concentration in Chemical Engineering from UNISA. Prior to joining the Powder Technology Group at UNISA, he worked as a research assistant at the SUT, focusing on additive manufacturing and welding. Sina's research interests encompass particle characterization, powder flow, and powder behaviour for powder bed Fusion methods, as well as the development of computational approaches using the Discrete/Finite Element methods.

Dr. Diego Barletta is Associate Professor of Chemical Engineering at the Department of Industrial Engineering of the University of Salerno. Member and from 2020 elected Chairman of the Working Party on Mechanics of Particulate Solids of the European Federation of Chemical Engineering. Member of editorial board of international journals (*KONA, Processes, Powders*) and of scientific committees of international conferences. Involved in research projects (FECUNDUS, MATHEGRAM, TUSAIL) funded by the European Commission. He is engaged in experimentally based research on mechanics of particulate solids, flow properties of powders at process conditions and on design and optimisation of biorefineries and of chemical processes with reduced CO_2 emissions.

Prof. Massimo Poletto is a Professor of Chemical Engineering at the Department of Industrial Engineering of the University of Salerno and has been a Guest Professor at East China University of Science and Technology Shanghai (2016–2022). Member and past Chairman of the Working Party Mechanics of Particulate Solids of the European Federation of Chemical Engineering. Subject editor (Powder technology) of Chemical Engineering Research and Design. He is presently involved in research concerning the study of flow properties of powders and particulates, including lignocellulosic biomass, fluidization and flow of cohesive powders, and powder spreading in the laser sintering process.